

# **BioRT-Flux-PIHM v1.0: a watershed biogeochemical reactive transport model**

Wei Zhi<sup>1</sup>, Yuning Shi<sup>2</sup>, Hang Wen<sup>1</sup>, Leila Saberi<sup>3</sup>, Gene-Hua Crystal Ng<sup>3</sup>, Kayalvizhi  
Sadayappan<sup>1</sup>, Devon Kerins<sup>1</sup>, Bryn Stewart<sup>1</sup>, Li Li<sup>1,\*</sup>

<sup>1</sup> Department of Civil and Environmental Engineering, The Pennsylvania State University, State  
College, PA 16802, USA

<sup>2</sup> Department of Ecosystem Science and Management, The Pennsylvania State University, State  
College, PA 16802, USA

<sup>3</sup> Department of Earth and Environmental Sciences, University of Minnesota, Twin Cities, MN  
55455, USA

\* Correspondence to [lili@engr.psu.edu](mailto:lili@engr.psu.edu)

## Abstract

Watersheds are the fundamental Earth surface functioning unit that connects the land to aquatic systems. Many watershed-scale models represent hydrological processes but often lack the representation of multi-component reactive transport processes that are relevant to soil and aquatic biogeochemical reactions. The lack of mechanism-based representation of reaction thermodynamics and kinetics at the watershed scale has limited our ability to understand and predict solute export and water quality, particularly under changing climate and anthropogenic conditions. Here we present a recently developed BioRT-Flux-PIHM (BioRT hereafter) v1.0, a watershed-scale biogeochemical reactive transport model. Augmenting the previously developed RT-Flux-PIHM that integrates land-surface interactions, surface hydrology, and abiotic geochemical reactions (Bao et al., 2017, WRR), the new development enables the simulation of 1) biotic processes including plant uptake, soil respiration, and microbially mediated reactions such as carbon decomposition and nutrient transformation; and 2) shallow and deep water partitioning to represent surface, shallow groundwater, and deep groundwater interactions. The reactive transport part of the code has been verified against the widely used reactive transport code CrunchTope. BioRT-Flux-PIHM v1.0 has recently been applied to understand reactive transport processes in multiple watersheds under diverse climate, vegetation, and geological conditions. This paper briefly introduces the governing equations and model structure with a focus on new model developments. It also showcases one hydrology example that simulates shallow and deep water interactions, and two biogeochemical examples relevant to nitrate and dissolved organic carbon (DOC). These examples are illustrated in two simulation modes of varying complexity. One is the spatially lumped mode (i.e., two land cells connected by one river segment) that focuses on processes and average behavior of a watershed. Another is the spatially distributed mode (i.e., hundreds of cells) that includes details of topography, land cover, and soil property conditions. The spatially distributed mode can be used to understand the impacts of spatial structure and identify hot spots of biogeochemical reactions.

## 1. Introduction

Watersheds are the fundamental Earth surface units that receive and process water, mass, and energy (Li, 2019;Li et al., 2020;Ranalli and Macalady, 2010;Hubbard et al., 2018;Seyfried et al., 2018). Watershed processes include land surface interactions that regulate evapotranspiration and discharge, and water partitioning between shallow soil lateral flow going into streams versus downward flow and recharge into the deeper subsurface (Edwards et al., 2015) (Figure 1). Complex biogeochemical interactions also occur among soil, water, roots, and microbes, dictating gas effluxes (e.g., CO<sub>2</sub>) via soil respiration, export of solute products derived from chemical weathering and biogeochemical transformation (Fatichi et al., 2019;van der Velde et al., 2010;Grathwohl et al., 2013).

These hydrological and biogeochemical processes determine how land surface responds to external forcings such as hydroclimatic drivers and human perturbations (van der Velde et al., 2014;Miller et al., 2020;Han et al., 2019;Steimke et al., 2018). Understanding these processes remains challenging due to the complex coupling of land surface processes, hydrology, and biogeochemical reactions (Kirchner, 2003). An example is the concentration-discharge (C-Q) relationships of solutes at stream and river outlets. These relationships encode the integrated signature of land surface responses to changes in hydrological conditions (Brooks et al., 2015;Zhi et al., 2020;Zhi and Li, 2020). Similar C-Q relationships have been observed for some solutes across watersheds under diverse geological and climatic conditions (Godsey et al., 2009;Basu et al., 2010;Moatar et al., 2017;Zarnetske et al., 2018;Godsey et al., 2019), whereas different solutes have shown contrasting patterns in the same watershed (Miller et al., 2017;Herndon et al., 2015;Zhi et al., 2019;Musolff et al., 2015). A general theory that can explain contrasting C-Q observations (e.g., flushing vs. dilution behaviors) under diverse watershed characteristics and forcing conditions remains elusive. The lack of understanding of mechanisms governing hydrological and biogeochemical interactions presents major roadblocks for forecasting water quality, including water issues such as eutrophication that persist worldwide.

One of the challenges to answering questions relevant to water quality and biogeochemical reactions is the lack of modeling tools that mechanistically link hydrological and biogeochemical processes at the watershed scale. Model development has been advancing separately within the disciplinary boundaries of hydrology and biogeochemistry (Li, 2019). Hydrologic models focus on solving for water storage and fluxes at the watershed scale and beyond (Fatichi et al., 2016). Reactive transport models (RTMs) have traditionally centered on transport and multi-component biogeochemical reactions typically in groundwater systems, which often have limited interactions with climate and other surficial watershed processes (Steefel et al., 2015; Li et al., 2017b; Mayer et al., 2002). Biogeochemical reactions in shallow soils that are often driven by environmental factors such as soil temperature and moisture cannot be well simulated in these models.

Previous modeling works has shown some integration across these two lines. For example, SWAT (Soil & Water Assessment Tool) (Gassman et al., 2007; Lam et al., 2010; Moriasi et al., 2013; Neitsch et al., 2011) includes a version that couples with the groundwater model MODFLOW and simulates surface water and groundwater quality in RT3D (Bailey et al., 2017; Ochoa et al., 2020). CATHY (Catchment Hydrology) includes processes of pesticide decay (Gatel et al., 2019; Scudeler et al., 2016). Some other hydrological models, including Hydrologiska Byråns Vattenbalansavdelning (HBV) and the Hydrological Predictions for the Environment (HYPE), also have modules that simulate processes relevant to nutrients and contaminants (Lindström et al., 2005; Lindström et al., 2010). While many of these models can simulate reaction processes such leaching of nutrients from agriculture lands (Lindström et al., 2005; Lindström et al., 2010; Bailey et al., 2017), most of them do not explicitly solve the multi-component reactive transport equations. In other words, they have relatively crude representations of solute leaching out of element bulk mass as part of the solute export but do not represent kinetics and thermodynamics of multi-component biogeochemical reactions typically included in reactive transport models (RTMs). They also do not simulate processes such as chemical weathering. As an example, nutrient leaching is often calculated based on empirical equations without explicitly solving reactive transport equations. Reaction rates are often represented using first-order decay (Gatel et al.,

2019), assuming reaction rate constants do not change with time and environmental conditions. However, biogeochemical processes including carbon decomposition and nutrient cycling are highly variable in space and time, depending on local environments such as substrate availability, soil temperature, and soil moisture (Li et al., 2017a; Suseela et al., 2012; HARTLEY et al., 2007). In filling in this model need, recently we augmented our watershed model RT-Flux-PIHM (Bao et al., 2017) with new developments of microbially mediated reactions, which allows us to model the interactions between biogeochemical reactions and environmental factors that are driven by land surface and hydrological processes.

This manuscript introduces BioRT-Flux-PIHM (BioRT hereafter) v1.0, augmented based on RT-Flux-PIHM with two new additions. One is the capability of simulating biotic processes including plant uptake of nutrients, soil respiration, and microbially mediated reactions in the soil. Examples include the soil respiration that produces CO<sub>2</sub> and carbon decomposition that generates dissolved organic carbon (DOC), and other nutrient transformation processes such as nitrification and denitrification. The other is the introduction of an optional deeper layer below the shallow soil that enables the simulation of interactions of deep water and shallow soil water flow (Figure 1). Here the deep water is loosely defined as the water beyond the soil zone, typically in less weathered, fractured subsurface that harbors relatively old and slow-moving groundwater contributing to streams. This contrasts with shallow water in highly permeable soils. Mounting evidence in recent years has shown that deeper water beyond the shallow soil interacts with streams, introduces water with distinct chemistry, sustains base flow in dry times, and buffers climate variability (Gurdak, 2017; Green, 2016; Taylor et al., 2013; Condon et al., 2013; Anyah et al., 2008; Maxwell et al., 2011; Gleeson et al., 2015). Stream chemistry often reflects the distinct chemistry from the shallow soil and deeper groundwater zones, i.e., the so called Shallow and Deep Hypothesis (Zhi et al., 2019; Zhi and Li, 2020). Deeper groundwater is thus a fundamental component of the hydrologic cycle and water budget. The groundwater-surface water interactions can also modulate land-atmospheric energy exchanges and soil moisture dynamics (Keune et al., 2016; Martínez-de la Torre and Miguez-Macho, 2019). Including the deep water component thus enables the simulation of such interactions and the dynamics of water quality.

This paper introduces new developments in the BioRT model. The code has been verified against the widely used reactive transport code CrunchTope (Supporting Information, SI). This paper briefly overviews water and energy related processes incorporated in the model. Readers are referred to previous publications for more details of processes such as evapotranspiration (ET), hydrological flow, and abiotic reactions (Shi et al., 2013; Bao et al., 2017; Li et al., 2017a; Qu and Duffy, 2007). We showcase three examples that illustrate the new model capabilities and the simulation of biogeochemical reactions. The first hydrological example shows the surface water and groundwater interactions. This second example focuses on nitrate transformation and transport in a spatially lumped mode. The third example examines the production and export of DOC with the representation of spatial details. The source code and the examples shown here are hosted on the GitHub website (<https://github.com/PSUmodeling/BioRT-Flux-PIHM>).

## **2. Model overview**

BioRT-Flux-PIHM integrates three modules (Figure 1). The Flux module is for land-surface processes including surface energy balance, solar radiation, and ET (Shi et al., 2013). The hydrology module PIHM simulates water processes including precipitation, interception, infiltration, recharge, surface runoff, subsurface lateral flow, and deep water flow (Qu and Duffy, 2007). The BioRT module simulates solute transport, bio-relevant processes such as plant uptake of nutrients from water, and multi-component reactions. The reaction processes can include soil respiration, microbially mediated redox reactions (e.g., soil respiration, carbon decomposition and nutrient transformation), ion exchange, aqueous and surface complexation, and mineral dissolution and precipitation. Note that geochemical reactions in our previous RT-Flux-PIHM are abiotic (Bao et al., 2017), including mineral dissolution and precipitation, aqueous and surface complexation, and ion exchange reactions.

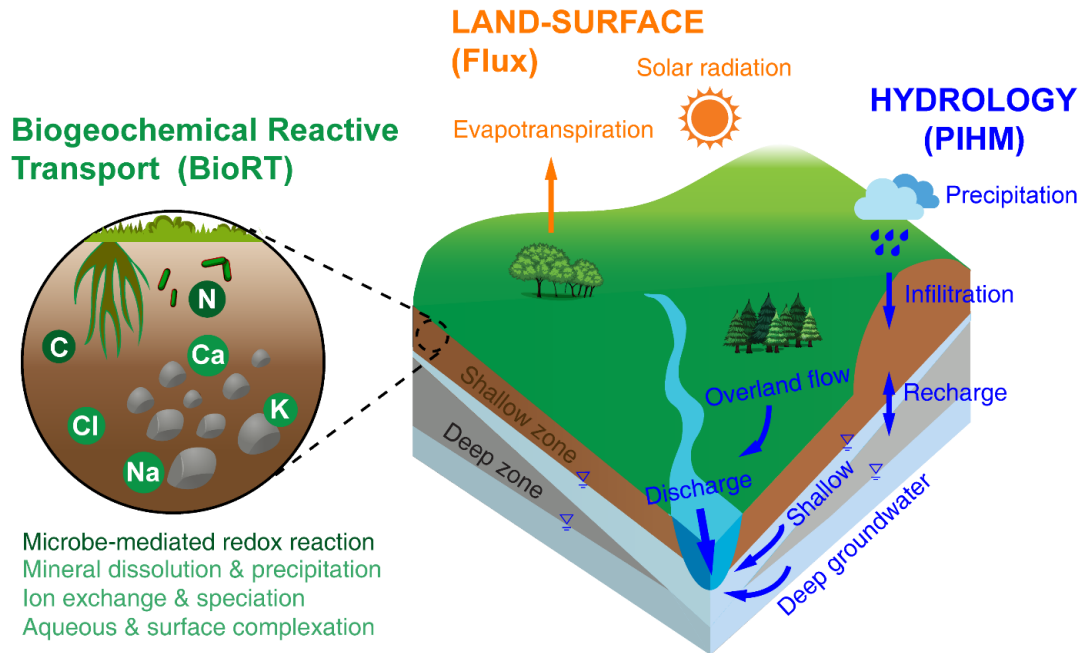


**Figure 1.** A conceptual diagram for processes at the watershed scale. This includes land surface interactions such as energy balance, solar radiation, evapotranspiration (e.g., evaporation, transpiration, and snow sublimation); hydrological processes partitioning water between surface runoff, shallow soil water, and deeper water entering the stream. Soil biogeochemical reactions include abiotic reactions (e.g., mineral dissolution and precipitation, ion exchange, surface complexations), and biotic processes such as soil respiration, plant uptake of nutrients, and other microbe-mediated reactions such as transformation of carbon and nitrogen. These processes are represented in three modules: The Flux module for land-surface interactions, the PIHM module for catchment hydrology, and the recently augmented BioRT module for biogeochemical reactions. Conceptually the shallow zone is the shallow soil and weathered zone that are more conductive to water flow (e.g., soil lateral flow or interflow). The deep zone refers to the less weathered zone that often harbors the relatively old and slow flowing groundwater. Reactions can occur in both shallow and deep zones. For the BioRT, the light and dark greens refer to abiotic and biological reactions, respectively.

The land surface and hydrology modules solve for soil temperature and water storage, from which water fluxes can be quantified for surface runoff, shallow and deep water fluxes. The BioRT module uses the calculated soil temperature, water storage, and water fluxes to simulate advection, diffusion/dispersion, and biogeochemical reactions in both shallow and deep zones (see governing equations in later sections). The reactions can be kinetically controlled (e.g., microbial redox reaction) or equilibrium-controlled (e.g., ion exchange, surface complexation (sorption), and aqueous complexation). Users can

define the types of reactions to be included and the form of reaction kinetics in input files. The output of BioRT includes the spatial distribution and time series of aqueous and solid concentrations, from which we can also infer reaction rates.

The simulation domain is structured as prismatic grids based on topography. Each grid is partitioned into surface and shallow and deep subsurface layers. The surface layer calculates water flow above ground (surface runoff). The shallow zone is loosely defined as the highly permeable subsurface that is contrasting to the deep zone that is broadly defined as the lower permeability zone beyond the shallow zone. In many places, this shallow zone is the soil zone that is most conductive to water flow (e.g., soil lateral flow) and is responsive to hydroclimatic forcings. The deep subsurface zone is the less weathered layer that harbors the relatively older and slower flowing ground water that contributes to stream flow. Note that these definitions differ from those in the hydrology community, which often refers to the shallow soil water flow or lumped shallow soil as groundwater, in a way that distinguishes it from the surface runoff (Winter et al., 1998;Dingman, 2015;Todd and Mays, 2005). These shallow and deep waters often have distinct solid and water chemistry, and are dominant at different time of the year, as have been observed and inferred in many catchments and watersheds (Brantley et al., 2018;Zhi et al., 2019;Zhi and Li, 2020;Li et al., 2020;Sullivan et al., 2016). Despite the model complexity, the model is flexible for taking inputs from online data portals or local measurements and it can accommodate low data availability (see the following section of 5 for data need and domain setup). The model is developed as a research tool to understand coupled watershed processes rather than as a policy model to guide management.

### **3. Governing equations and processes**



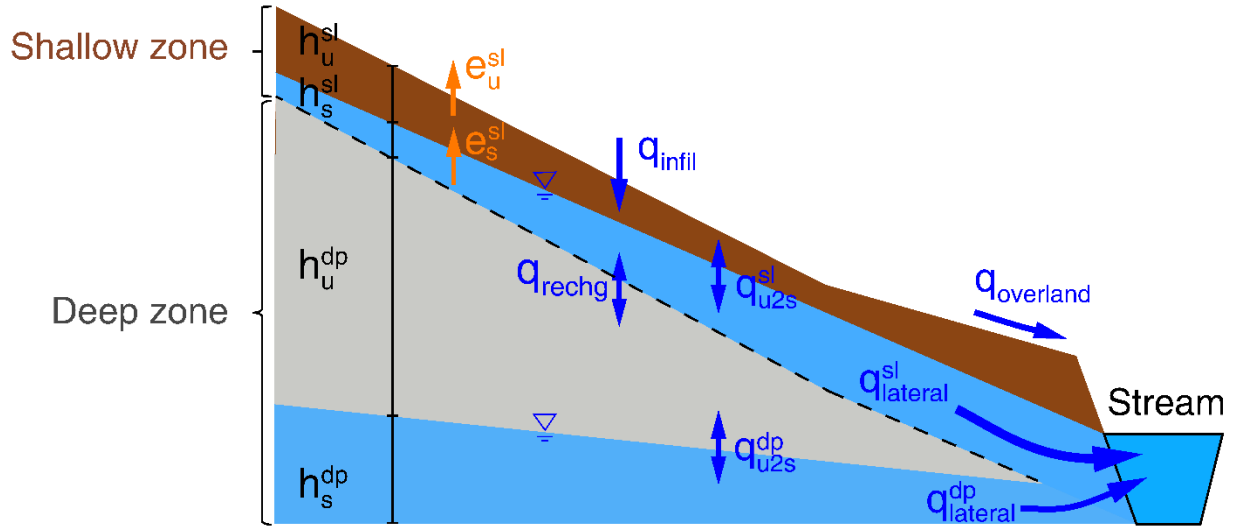


**Figure 2.** Hillslope view of the shallow and deep zones and relevant water flows. The symbol of “h”, “e”, and “q” denotes water storage [m], evapotranspiration [m/s], and water flow [m/s], respectively. The superscript letter “sl” and “dp” refer to shallow and deep zone, respectively. The subscript letters “u” and “s” refer to unsaturated and saturated layer, respectively. Detailed equations are listed in the following sections. The terms “infil”, “u2s”, and “recharge” refer to infiltration, unsaturated to saturated zones, and recharge.

### 3.1 Water equations

The original Flux-PIHM simulates surface runoff and a lumped subsurface flux into streams without distinguishing shallow soil water flow and deeper groundwater flow. In working with stream water chemistry data, we realized that a lumped subsurface flow cannot describe the dynamics of stream chemistry, as the shallow soil water and deeper groundwater have distinct chemistry and are dominant at different times of the year (Zhi et al., 2019; Zhi and Li, 2020). We therefore added an optional deeper groundwater zone in the code to simulate the deeper water that interacts with streams. Each prismatic element now has three zones in the vertical direction: surface (or above ground), shallow and deep zones in the subsurface.

In each prismatic element  $i$ , the shallow zone includes unsaturated and saturated water storages. The unsaturated zone receives water from the surface via infiltration and only flows vertically to the saturated zone. The saturated zone flows both vertically to the

deep zone (recharge) and laterally to neighboring grids  $j$  or the stream (lateral). The code solves the following equations for the shallow zone:

$$\theta_i^{sl} \frac{dh_{i,u}^{sl}}{dt} = q_{i,inf} - q_{i,u2s}^{sl} - e_{i,u}^{sl} \quad (1)$$

$$\theta_i^{sl} \frac{dh_{i,s}^{sl}}{dt} = q_{i,u2s}^{sl} - q_{i,rechg} - e_{i,s}^{sl} + \sum_1^{N_{ij}} q_{ij}^{sl} \quad (2)$$

Where  $\theta_i^{sl}$  [m<sup>3</sup> pore space/m<sup>3</sup> total volume] is the shallow zone porosity in the element  $i$ ;  $h_{i,u}^{sl}$  and  $h_{i,s}^{sl}$  [m] are the unsaturated and saturated water storage in the shallow zone, respectively. Note that the storages  $h$  here are essentially the height of soil column with equivalent saturated water, not the height of the pure water (100% volume) column. That is why porosity is in the equation. For saturation zones, this height is needed to quantify the depths of water tables and determines the direction of water flow between neighboring grids. The  $q_{i,inf}$  [m/s] is the infiltration rate from the surface to the shallow zone;  $q_{i,u2s}^{sl}$  [m/s] is the vertical flow from the unsaturated layer to the saturated layer in the shallow zone;  $q_{i,rechg}$  [m/s] is the recharge rate from the shallow zone to the deep zone;  $e_{i,u}^{sl}$  and  $e_{i,s}^{sl}$  [m/s] are evapotranspiration (ET) from the unsaturated and saturated layer in the shallow zone, respectively;  $q_{ij}^{sl}$  [m/s] are the lateral flows in the shallow saturated layer between the element  $i$  and its neighbor element  $j$ ;  $N_{ij}$  ( $\leq 3$ ) is the number of neighbor elements  $j$ . For a prismatic element  $i$ , a boundary cell could have one or two neighbors; a non-boundary cell has three neighbors. The ET is calculated by the Penman potential evaporation scheme and detailed equations can be found in Shi (2012). A similar set of water equations for the deep zone are in the SI (Eqn. S1 and S2).

Infiltration and vertical fluxes from the unsaturated to the saturated layer in the shallow zone are based on the Richards equation, in which hydraulic water head  $H$  (i.e., the summation of water storage  $h$  and elevation head  $z$ ) and hydraulic conductivity  $K$  are used to determine the fluxes in each element  $i$ :

$$q_{i,inf} = K_{i,inf} \frac{H_{i,sur} - H_{i,u}^{sl}}{d_{i,inf}} \quad (3)$$

$$q_{i,u2s}^{sl} = K_{i,V}^{sl} \frac{H_{i,u}^{sl} - H_{i,s}^{sl}}{0.5d_i^{sl}} \quad (4)$$

Where  $d_{i,inf}$  and  $d_i^{sl}$  [m] are the thickness of infiltration layer and shallow zone depth for the elements  $i$ , respectively;  $K_{i,inf}$  [m/s] is the hydraulic conductivity of the infiltration layer, the top 0.1 m of the subsurface and is considered to have different conductivity from the rest of subsurface;  $K_{i,V}^{sl}$  [m/s] is the hydraulic conductivity in the vertical direction (i.e., weighted average of macropore  $K_{i,macV}$  and soil matrix  $K_{i,satV}$ , Eqn. S7);  $H_{i,sur}$  [m] is the surface hydraulic water head ( $= h_{i,sur} + z_{i,sur}$ );  $H_{i,u}^{sl}$  and  $H_{i,s}^{sl}$  [m] are the shallow hydraulic water heads in the unsaturated and saturated layer, respectively. The lateral flow in the shallow saturated layer is calculated using Darcy's law:

$$q_{ij}^{sl} = K_{ij}^{sl} \frac{H_{i,s}^{sl} - H_{j,s}^{sl}}{d_{ij}} \quad (5)$$

Where  $d_{ij}$  [m] is the distance between the centers of elements  $i$  and  $j$ ;  $K_{ij}^{sl}$  [m/s] is the harmonic mean of shallow hydraulic conductivity in the horizontal direction between elements  $i$  ( $K_{i,H}^{sl}$ ) and  $j$  ( $K_{j,H}^{sl}$ ). The interaction between the shallow saturated zone and stream channel also follows Eqn. 5, except that the adjacent head is replaced by the level of the channel water. Similar to the shallow zone, hydrological equations in the deep zone are detailed in the SI (Eqn. S1 – S8).

267

### 268 **3.2 Reactive transport equations**

269 The governing advection dispersion reaction (ADR) equation for an arbitrary solute  
270  $m$  in grid  $i$  is as follows (Bao et al., 2017), i.e., the change of solute mass (i.e., the left  
271 term in Eqn. 6) is driven by dispersive transport, advective transport, and reactions (i.e.,  
272 the 1<sup>st</sup>, 2<sup>nd</sup>, and 3<sup>rd</sup> right-hand side terms, respectively):

$$V_i \frac{d(S_{w,i}\theta_i C_{m,i})}{dt} = \sum_1^{N_{ij}} \left( A_{ij} D_{ij} \frac{C_{m,j} - C_{m,i}}{d_{ij}} - q_{ij} A_{ij} C_{m,j} \right) + R_{m,i}, \quad m = 1, \dots, nm \quad (6)$$

274 Where  $V_i$  [m<sup>3</sup> total volume] is the total volume of element  $i$ ;  $S_{w,i}$  [m<sup>3</sup> water/m<sup>3</sup> pore space]

is soil water saturation;  $\theta_i$  [ $\text{m}^3$  pore space/ $\text{m}^3$  total volume] is porosity;  $C_{m,i}$  [ $\text{mol}/\text{m}^3$  water] is the aqueous concentration of species  $m$ ;  $N_{ij}$  is the number of fluxes from neighbor element  $j$  for element  $i$ ,  $N_{ij}$  is 2 for the unsaturated zone (infiltration, recharge) with only vertical flows and 5 for saturated zone with flux from (or to) the unsaturated zone, from (or to) the deeper zone, and fluxes between  $i$  and three neighbor elements  $j$  in lateral flow directions for non-boundary grids;  $A_{ij}$  [ $\text{m}^2$ ] is the grid area shared by  $i$  and its neighbor grid  $j$ ;  $D_{ij}$  [ $\text{m}^2/\text{s}$ ] is the hydrodynamic dispersion coefficient (i.e., sum of mechanical dispersion and effective diffusion coefficient) normal to the shared surface  $A_{ij}$ ;  $d_{ij}$  [ $\text{m}$ ] is the distance between the center of  $i$  and its neighbor elements  $j$ ;  $q_{ij}$  [ $\text{m}/\text{s}$ ] is the flow rate across  $A_{ij}$ ;  $R_{m,i}$  [ $\text{mol}/\text{s}$ ] is the total rate of kinetically controlled reactions in element  $i$  that involve species  $m$ ;  $nm$  is the total number of independent primary species to be solved for reactive transport equations.

### 3.3 Biogeochemical processes and reaction kinetics

#### 3.3.1 Biogeochemical processes

Here we discuss some representative biogeochemical processes that involve plants and microbes that can be included in BioRT. BioRT differs from general water quality models that often primarily target a few contaminants (e.g., N, P, metals). The framework of the code is flexible and the users can define their reactions and solutes of interests in the input files. For abiotic reactions such as mineral dissolution and surface complexation or ion exchange, readers are referred to an earlier paper (Bao et al. (2017)). Generally speaking, shallow soils compared to deep soils contain more weathered materials and soil organic matters (SOM) including roots, leaves, and microbes. SOM can be decomposed partially into organic molecules that dissolve in water (Wieder et al., 2015), i.e., DOC, or it can be oxidized completely into  $\text{CO}_2$  that is released back to the atmosphere as a gas (Davidson, 2006) or surface water in the form of dissolved inorganic carbon (DIC). With coexisting cations (e.g., Ca, Mg), DIC can often precipitate and become carbonate minerals (e.g.,  $\text{CaCO}_3$ ).

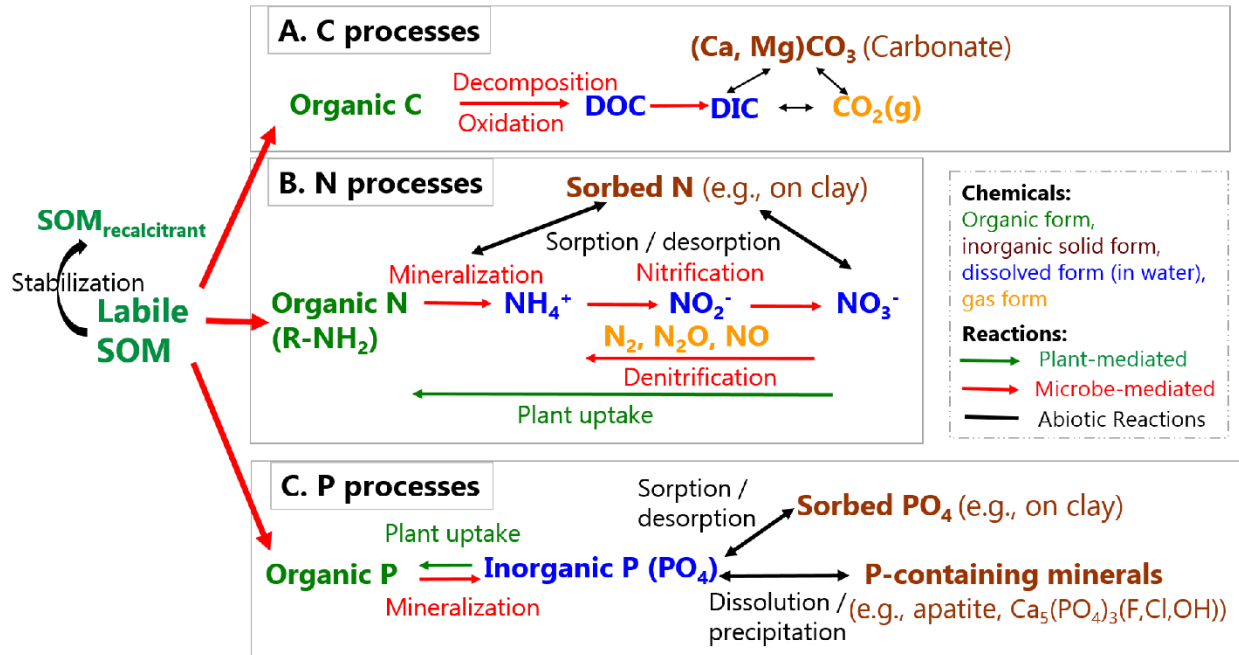


**Figure 3.** Biotic and abiotic reactions relevant to the transformation of soil organic matter (SOM). It can become stabilized through sorption on clay and separation from reactants. Labile OM can decompose into inorganic forms, releasing C, N, and P that further transform between different forms (adopted from Li (2019), permission with Mineralogical Society of America).

OM decomposition releases organic nitrogen ( $\text{R-NH}_2$ ), which can further react to become  $\text{NH}_4^+$ , and other nitrogen forms ( $\text{N}_2$ ,  $\text{N}_2\text{O}$ ,  $\text{NO}$ ,  $\text{NO}_2^-$ ,  $\text{NO}_2$ ) (Figure 3). The gases can be emitted back to the atmosphere (Saha et al., 2017; Maavara et al., 2018). Denitrification requires anoxic conditions and occurs less commonly in shallow soils owing to the pervasive presence of  $\text{O}_2$  (Sebestyen et al., 2019); it can become important under wet conditions and in  $\text{O}_2$ -depleted groundwater systems. Phosphorous (P) can be in an organic form (e.g., leaves), sorbed on fine soil particles, dissolved in water, or in solid forms as P-containing minerals. Transformation of nutrients occurs through various bio-mediated or abiotic reactions. A representative P-containing mineral in the Earth's crust is apatite  $\text{Ca}_5(\text{PO}_4)_3(\text{F}, \text{Cl}, \text{OH})$ . Once liberated via rock dissolution, P is mostly biologically assimilated and locked in organic forms. These organic forms have very low solubility, allowing them to bind on and be transported together with soil particles in the form of orthophosphate or pyro-diphosphate. Overall, these reactions are a combination of biotic and abiotic reactions.

### 3.3.2 Reaction kinetics in natural soils

**Rate dependence on temperature and soil moisture.** Reactions such as soil respiration and plant uptake typically depend on environmental conditions (temperature or soil moisture). For example, in shallow oxic soils where organic carbon and  $O_2$  are often abundant, the rate law for carbon decomposition can be simplified to the following form assuming microorganism concentrations are relatively constant.

$$r = kAf(T)f(S_w)f(Z_w) \quad (7)$$

Where the reaction rate  $r$  [mol/s] depends on rate constant  $k$  [mol/m<sup>2</sup>/s], the surface area  $A$  [m<sup>2</sup>] is a lumped parameter that quantitatively represents SOM content and biomass abundance,  $f(T)$  and  $f(S_w)$  describe the temperature and soil moisture dependence, respectively,  $f(Z_w)$  can be included to account for the depth distribution of SOM (Seibert et al., 2009), and  $Z_w$  [m] is the water table depth. An example for the depth distribution is  $f(Z_w) = \exp\left(-\frac{Z_w}{b_m}\right)$  (Weiler and McDonnell, 2006;Ottoy et al., 2016;Bai et al., 2016), with  $b_m$  as the depth coefficient describing the gradient of SOM content over depth. Users can choose to include either one or all of these dependences in input or database files.

The temperature dependence follows a  $Q_{10}$ -based form (Friedlingstein et al., 2006;Hararuk et al., 2015) as follows:

$$f(T) = Q_{10}^{|T-20|/10} \quad (8),$$

where  $Q_{10}$  is the relative increase in reaction rates when temperature increases by 10 °C (Davidson and Janssens, 2006). Values of  $Q_{10}$  (Figure 4a) can vary from 1.0 to 3.0, depending on climatic conditions, substrate availability, and ecosystem type (e.g., grassland, forest) (Davidson et al., 2006;Liu et al., 2017). The mean values are in the range of 1.4 to 2.5 (Zhou et al., 2009;Bracho et al., 2016). The  $Q_{10}$  value can be specified in the input file. The soil moisture dependence function  $f(S_w)$  is coded based on the following form:

$$\begin{cases} \left(\frac{S_w}{S_{w,c}}\right)^n, S_w \leq S_{w,c} \\ \left(\frac{1-S_w}{1-S_{w,c}}\right)^n, S_w > S_{w,c} \end{cases} \quad (9)$$

Here  $S_{w,c}$  [0 to 1] is the critical soil moisture at which rates are highest, and  $n$  is the exponent reflecting the dependence of rates on soil moisture. A typical  $n$  value is 2 (Yan et al., 2018) with a range between 1.2 and 3.0 (Hamamoto et al., 2010), depending on soil structure and texture. As shown in Figure 4b, the form indicates an intermediate critical soil moisture  $S_{w,c}$  at which  $f(S_w)$  reaches its maximum. When  $S_w$  is below this value,  $f(S_w)$  increases with  $S_w$ ; when  $S_w$  is above this value,  $f(S_w)$  decreases with  $S_w$  behavior (Figure 4b) (Yan et al., 2018). Under the extreme conditions of  $S_{w,c}$  equals to 0 or 1,  $f(S_w)$  monotonically increase or decrease (Figure 4c). The two parameters,  $S_{w,c}$  and  $n$ , determines the shape of the curve. They can be specified in input or database files. One can also choose not to have temperature or soil moisture dependence by choosing parameters that would lead to the value of exponent being zero.

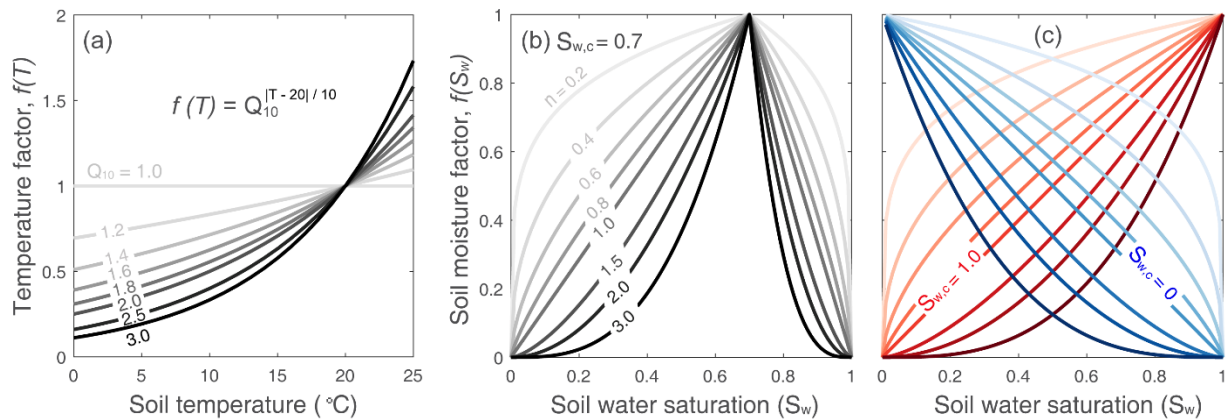


**Figure 4.** (a) Function form of soil temperature dependence and (b, c) soil moisture dependence for reaction rates. The temperature factor  $f(T)$  is a function of the  $Q_{10}$  (defined by users) and soil temperature. The soil moisture factor  $f(S_w)$  is a function of two user-defined parameters  $S_{w,c}$  and  $n$  and soil water saturation  $S_w$ . The soil moisture function can represent three types of behaviors: the threshold behavior (b,  $0 < S_{w,c} < 1$ ), increase behavior (red in (c),  $S_{w,c} = 1$ ), and decrease behavior (blue in (c),  $S_{w,c} = 0$ ). Values of  $n = 1$  leads to a linear threshold dependence of  $S_w$  while  $n < 1$  and  $n > 1$  lead to concave and convex dependences, respectively.

**Rate dependence on substrates: Monod kinetics and biogeochemical redox ladder.** Deeper groundwater aquifers often experience anoxic conditions that lead to processes such as denitrification or methanogenesis. This can also happen in wetlands or wet soils. The rates of microbe-mediated redox reactions depend not only on temperature and soil moisture as discussed above, they also depend on concentrations

of electron donors and non-oxygen electron acceptors (e.g., nitrate, iron oxides, sulfate) that are often limited under anoxic conditions (Bao et al., 2014; Li, 2019). The order of the redox reactions often follows the biogeochemical redox ladder, which is based on how much microbe can harvest energy by reducing different types of electron acceptors. Monod reaction rate laws are often used for quantifying rates of these redox conditions. These rate laws are detailed in the section S2 of Supporting Information and also in Li (2019). Users can combine these Monod rate laws and the temperature and soil moisture dependence described above, if needed.

### 3.4 Plant related processes: root uptake of nitrate as an example

Nitrate uptake by plants is intrinsically complex and remains poorly understood (Devienne-Barret et al., 2000; Crawford and Glass, 1998; Hachiya and Sakakibara, 2016). A variety of plant uptake models exists with varying degrees of complexity (Neitsch et al., 2011; Fisher et al., 2010; Cai et al., 2016). These models are mostly based on plant growth module or supply and demand approach that often requires detailed phenological and plant attributes such as growth cycle, root age and biomass, nitrate availability, phosphorous stress, and carbon allocation, in addition to local climate conditions such as temperature and soil moisture (Neitsch et al., 2011; Porporato et al., 2003; Dunbabin et al., 2002; Buysse et al., 1996; Fisher et al., 2010). Without detailed information, we can assume a simple and operational approach (Eqn. 13 and 14). In the Example 2 that we show later, for example, we modeled nitrate uptake with dependence on  $\text{NO}_3^-$  concentration, soil temperature and moisture, and rooting density (McMurtrie et al., 2012; Yan et al., 2012; Buljovic and Engels, 2001).

$$r_{\text{uptake}} = k_{\text{uptake}} C_{\text{NO}_3^-} f(T) f(S_w) f_{\text{root}}(d_w) \quad (13)$$

$$f_{\text{root}}(d_w) = \exp((-d_w + \delta) / \lambda) \quad (14)$$

Where  $k_{\text{uptake}}$  [L/s] is the nitrate uptake rate,  $f_{\text{root}}(d_w)$  is the normalized rooting density term in the range of 0 to 1 as a function of water depth to the groundwater ( $d_w$ ). The rooting term (Eqn. 14) was exponentially fitted ( $\delta = 0.013, \lambda = 0.20$ ) based on field measurements of root distribution along depth (Hasenmueller et al., 2017). It is common to observe root density decrease exponentially in forests (López et al., 2001). Other form



of user-tailored plant uptake rate law can be added if needed.

#### 4. Numerical scheme and model verification

The system of differential equations for the water storages (e.g., Eqn. 1 and 2, and Eqn. S1 and S2) are assembled into a global system of ordinary differential equations (ODEs) and solved in CVODE (short for C-language Variable-coefficients ODE solver, <https://computing.llnl.gov/projects/sundials/cvode>), a numerical ODE solver in the SUite of Nonlinear and Differential / ALgebraic equation Solvers (SUNDIALS) (Hindmarsh et al., 2005). In BioRT, the transport step is first solved with water by the preconditioned Krylov (iterative) method and the Generalized Minimal Residual Method (Saad and Schultz, 1986). In the following reaction step, all primary species in each finite volume are assembled in a local matrix and then solved iteratively by the Crank-Nicolson and Newton-Raphson method in CVODE (Bao et al., 2017).

**Model verification.** The BioRT module had been verified against CrunchTope under different transport and reaction conditions (Figures S1 – S7 in SI). CrunchTope is a widely used subsurface reactive transport model (Steefel and Lasaga, 1994; Steefel et al., 2015), and is often used as a benchmark to verify other reactive transport models. Verification was performed under simplified hydrological conditions with 1-D column and constant flow rates such that it focuses on advection, diffusion, dispersion, and biogeochemical reactions. Specifically, three cases of soil phosphorus, carbon, and nitrogen were verified for temporal evolution and spatial pattern of relevant solute concentrations. The phosphorus case that involves kinetics-controlled apatite dissolution and thermodynamics-controlled phosphorous speciation was first tested for solution accuracy of the bulk code that was inherited from the original RT-Flux-PIHM. Soil carbon and nitrogen processes that involve microbe-driven processes, such as soil carbon decomposition and mineralization, nitrification and denitrification, were further verified for solution accuracy of the augmented BioRT module.

#### 5. Model structure, data needs, and domain setup

**Model structure.** The model takes meteorological forcing time series as input and solves for water storages and soil temperature, along with other hydrologic and land surface states and fluxes (Figure 5). BioRT reads in the model output of water and temperature from Flux-PIHM, and solves the biogeochemical reactive transport equations. At the time scale of months to years that are typical for BioRT-Flux-PIHM simulations, alterations in solid phase properties, including, porosity, permeability, and reactive surface area, are considered negligible such that hydrological parameters remain constant with time.

**Data needs.** The code sets up the model domain based on watershed characteristics including topography, land cover, and shallow and deep zone properties (Figure 5). When the model is used in a spatially distributed form, the model domain can be set up using elevation, land cover, soil and geology maps supplied by the user or from the data portal of Geospatial Data Gateway (<https://datagateway.nrcs.usda.gov>). The meteorological forcing data can be downloaded from the North American Land Data Assimilation Systems Phase 2 (NLDAS-2, <https://ldas.gsfc.nasa.gov/nldas/v2/forcing>). The vegetation forcing, i.e., Leaf Area Index (LAI), can be obtained from MODIS (Moderate Resolution Imaging Spectroradiometer, <https://modis.gsfc.nasa.gov/data>). Other vegetation properties associated with land cover (e.g., shading fraction, rooting depth) can be adopted from, for example, the Noah vegetation parameter table embedded in the Weather Research and Forecasting model (WRF; Skamarock and Klemp (2019)). Local measurements from meteorological stations and field campaigns (e.g., land cover, soil, geology) can also be used in the model. Another data source is the HydroTerre (<http://www.hydroterre.psu.edu/>), where users can obtain geospatial data (e.g., elevation, land cover, geology, soil) (Leonard and Duffy, 2013). Initial water and solid phase chemistry can be based on measurements or general knowledge of the simulated sites. The form of reaction rate laws, including the Monod form, temperature and soil moisture dependence, can be defined in the input files and calibrated to reproduce field data. Reaction thermodynamics, mostly equilibrium constants, are from the geochemical database EQ3/6 by default (Wolery, 1992). These reaction parameters can be modified when necessary. The model outputs include aqueous and solid concentrations of shallow and deep zone and stream water.

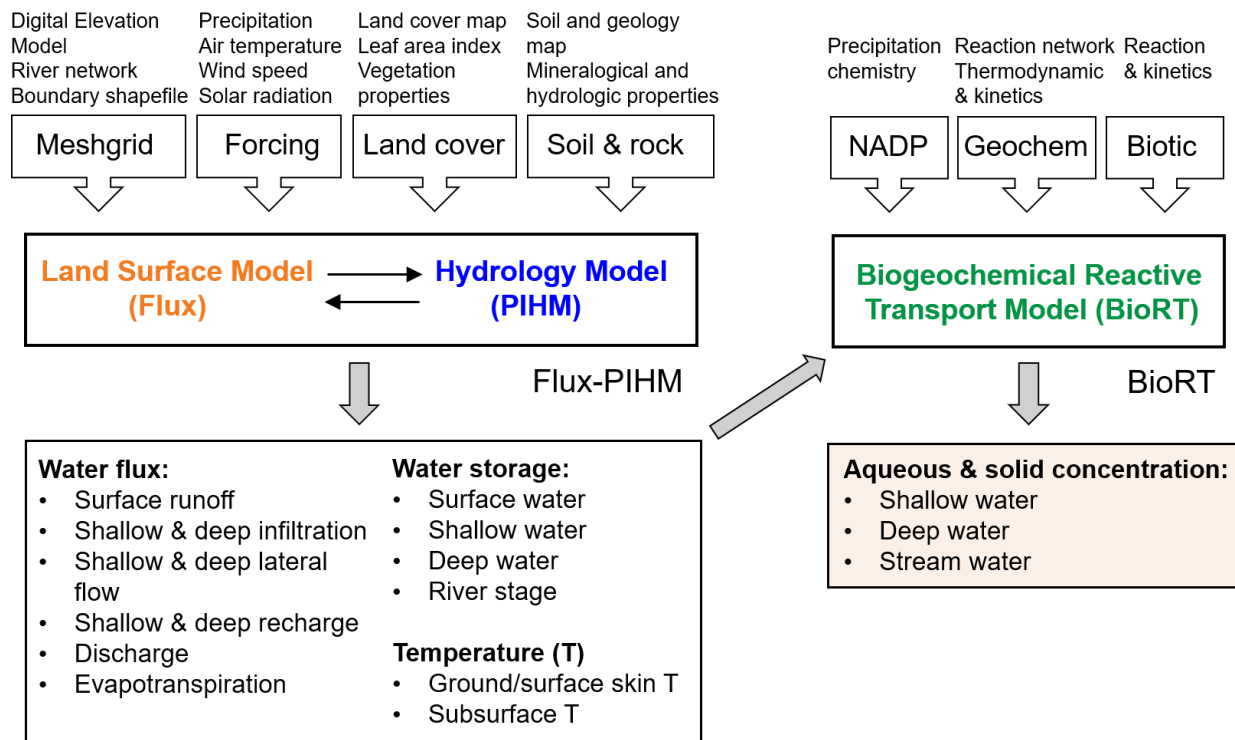


**Figure 5.** Model structure, input, and output of BioRT-Flux-PIHM. The Flux-PIHM takes in watershed characteristics including topography (digital elevation model, DEM), land cover, shallow and deep zone properties, and meteorological forcing time series and solves for water storage, and ground and soil temperature. BioRT takes in water- and temperature-related information from Flux-PIHM with additional inputs such as precipitation chemistry and shallow and deep water chemistry and biogeochemical kinetics parameters, and solve for aqueous and solid concentrations in the shallow and deep zone, and stream water. NADP stands for the National Atmospheric Deposition Program. This paper focuses on the BioRT component. The land-surface, hydrological processes, and abiotic reactive transport processes have been described in previous papers (Bao et al., 2017; Shi et al., 2013). Discussions on how air temperature and ET influence stream chemistry can be found in Li (2019).

**Domain set up: from simple, spatially lumped to complex, spatially distributed domains.** The domain can be set up at different spatial resolutions with different numbers of grids. A simple domain can be set up with only two land grids representing two sides of a watershed connected by one river cell. This setup uses averaged properties without needs for larger spatial data. Alternatively, a complex domain can be set up using many grids with explicit representation of spatial details. The model domain can be set up using PIHM-GIS ([http://www.pihm.psu.edu/pihmgis\\_home.html](http://www.pihm.psu.edu/pihmgis_home.html)), a standalone GIS interface for watershed delineation, domain decomposition, and parameter assignment (Bhatt et al.,

2014). It requires much more data and can be computationally expensive but can be used to identify “hot spots” of biogeochemical reactions within a watershed. The same model processes (e.g., hydrology, reaction network) can be setup in both spatial configurations. Auto-calibration is not built into the model, but a global calibration coefficient approach is used to reduce parameter dimension and facilitate manual calibration. A typical model application requires 20 to 30 hydrological parameters to be calibrated. These parameters include land surface parameters (e.g., canopy resistance, surface albedo), soil and geology parameters (e.g., hydraulic conductivity, porosity, Van Genuchten, macropore properties) (Shi et al., 2013). Reaction-related parameters (e.g., reaction rate constant, mineral surface area,  $Q_{10}$ ,  $S_{w,c}$ , and  $n$ ) are additionally needed for calibration, the number of which depends on the numbers of reactions involved in a particular system.

## 6. Model applications

The original RT-Flux-PIHM has been applied to understand processes related to the geogenic solutes of Cl and Mg at the Shale Hills watershed and for Na in a watershed on Volcán Chimborazo in the Ecuadorian Andes (Table 1). The new BioRT-Flux-PIHM has been demonstrated for understanding the dynamics of DOC and nitrate at Shale Hills and Coal Creek. This section will present one hydrology and two biogeochemical examples in the Susquehanna Shale Hills Critical Zone Observatory (SSHCZO), a small headwater watershed in central Pennsylvania, USA. The mean annual precipitation is approximately 1,070 mm and the mean annual temperature is 10 °C (Brantley et al., 2018). Soil carbon storage and respiration and nitrogen budget and fluxes have been studied in detail (Andrews et al., 2011; Hasenmueller et al., 2015; Shi et al., 2018; Hodges et al., 2019; Weitzman and Kaye, 2018). Modeling work has been conducted to understand hydrological dynamics (Shi et al., 2013; Xiao et al., 2019), transport of the non-reactive tracer Cl, and the weathering-derived solute Mg (Bao et al., 2017; Li et al., 2017a).

**Table 1.** Existing Model applications of BioRT-Flux-PIHM

Watershed (location)	Size (km <sup>2</sup> )	Model domain	Modeled solute	Reactions (rate laws: 1, TST; 2, Monod based; 3, plant uptake)	Reference
-------------------------	----------------------------	-----------------	-------------------	--	-----------

Shale Hills (PA, USA)	0.08	Spatially distributed	Cl, Mg	<ul style="list-style-type: none"> <li>• Chlorite dissolution<sup>1</sup></li> <li>• Illite dissolution<sup>1</sup></li> <li>• Carbonate dissolution &amp; precipitation<sup>1</sup></li> <li>• Cation exchange</li> </ul>	Bao et al., 2017; Li et al., 2017
		Spatially distributed	DOC	<ul style="list-style-type: none"> <li>• SOC decomposition<sup>2</sup></li> <li>• DOC sorption</li> </ul>	Wen et al., 2020
		Spatially lumped	NO <sub>3</sub> <sup>-</sup>	<ul style="list-style-type: none"> <li>• Soil N leaching<sup>2</sup></li> <li>• Denitrification<sup>2</sup></li> <li>• Plant uptake<sup>3</sup></li> </ul>	This work
Coal Creek (CO, USA)	53	Spatially lumped	DOC, Na	<ul style="list-style-type: none"> <li>• SOC decomposition<sup>2</sup></li> <li>• DOC sorption</li> <li>• Albite dissolution<sup>1</sup></li> </ul>	Zhi et al., 2019
Volcán Chimborazo (Ecuador)		Spatially distributed	Cl, Na, Ca, Mg, SiO <sub>2</sub>	<ul style="list-style-type: none"> <li>• Albite dissolution<sup>1</sup></li> <li>• Diopside dissolution<sup>1</sup></li> </ul>	Saberi et al. (under review)

Note: Transition State Theory (TST) is a classic kinetic rate law for mineral dissolution and precipitation (Brantley et al., 2008) (Eqn. S15); Monod rate law with environmental dependency (i.e., soil temperature and soil moisture) is widely used for microbially driven reactions. Monod-based and plant nitrate uptake rate law are detailed in the following section of 6.2. SOC stands for soil organic carbon.

## 6.1 Example 1: Shallow and deep water interactions

The model was set up using the spatially lumped mode with two land grids and one river grid characterized by average land cover, soil and rock properties based on previous work (Shi et al., 2013; Kuntz et al., 2011). The model assumed a Weikert soil, the dominant soil type at Shale Hills (Shi et al., 2013). The porosity of the deep zone was set to a tenth of the shallow soil porosity based on measurements of the groundwater aquifer (Brantley et al., 2018; Kuntz et al., 2011). In a headwater catchment like Shale Hills where the deep groundwater is most likely sourced from recharge, the deep groundwater contribution to the stream can be primarily controlled by the hydraulic conductivity ( $K_{satH}$ ) contrast between the deep and shallow zones (i.e.,  $K_{satH}^{dp} / K_{satH}^{sl}$ ). This is because the  $K_{satH}$  contrast determines the partitioning of infiltrating water between the shallow lateral flow and the downward recharge to the deep zone and then deep groundwater flow. Two cases of high (red) and low (blue)  $K_{satH}^{dp}$  were set up to showcase

the control of  $K_{satH}$  contrast on deep groundwater (Figure 6a). By changing the deep zone  $K_{satH}^{dp}$  from 2.6 to 0.22 (m/d), the annual deep groundwater ( $Q_G$ ) contribution to discharge ( $Q$ ) decreased from 26% to 5.2%, although the total discharge is negligible. This indicates that the changing  $K_{satH}^{dp}$  mostly changes the portioning between the shallow soil lateral flow and recharge, whereas total infiltration and discharge remain very similar.

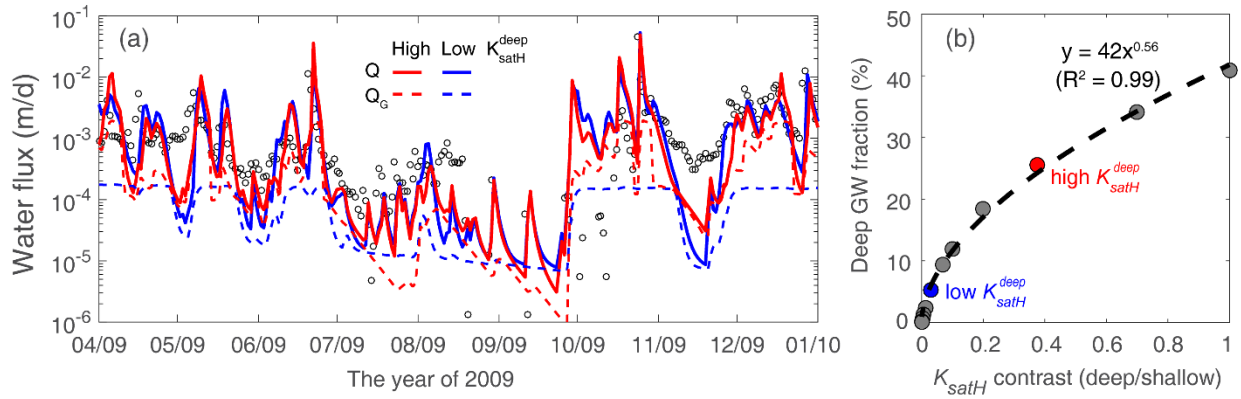


**Figure 6.** (a) Hydraulic conductivity ( $K_{satH}$ ) contrast control on deep groundwater ( $Q_G$ ). The cases of high ( $K_{satH}^{dp} = 2.6$  m/d, red) and low conductivity ( $K_{satH}^{dp} = 0.22$  m/d, blue) led to 26% and 5.2% of annual  $Q_G$  contribution to discharge ( $Q$ ), respectively. (b) Deep groundwater fraction as a function of  $K_{satH}$  contrast between the deep and shallow zone. The  $K_{satH}$  contrast was limited to 1 in the figure as most watersheds exhibit a smaller  $K_{satH}$  in the deep zone than in the shallow zone. The two red and blue dots correspond to the two cases in left panel.

Several additional cases were further tested to examine the relationship between deep groundwater fraction (%) of discharge and  $K_{satH}$  contrast. Figure 6b shows that the deep groundwater fraction rapidly increases with the increasing ratio of  $K_{satH}^{dp} / K_{satH}^{sl}$ , reaching a limit when  $K_{satH}$  contrast is sufficiently high. The deep groundwater contribution to the stream reaches  $\sim 40\%$  when the  $K_{satH}^{dp}$  and  $K_{satH}^{sl}$  are equal. In natural systems, we do see places, for example, karst formations, where groundwater contributes to more than 40% (Hartmann et al., 2014; Husic, 2018). These places may have higher deeper conductivity than shallow soils due to the development of highly conductive conduits.

## 6.2 Example 2: Nitrate dynamics in a spatially implicit domain

This example focuses on nitrate ( $\text{NO}_3^-$ ), a dominant dissolved N form in water with abundant measurements (<https://criticalzone.org/shale-hills/data/datasets/>) (Weitzman and Kaye, 2018). The N processes at Shale Hills include atmospheric N deposition, soil N leaching, stream export, denitrification, and plant uptake (Figure 7). Based on field measurements, the atmospheric deposition at the site is the dominant N input and N export via discharge is only a small fraction (2.5%) of atmospheric N input, indicating most deposited N is tightly cycled by plants or lost to the atmosphere via denitrification.

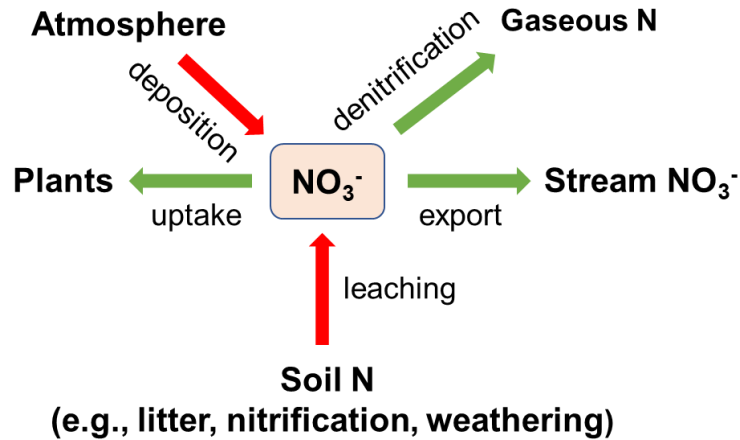


**Figure 7.** Modeled nitrogen processes in Example 2. Atmospheric N deposition is the major N input; denitrification and plant uptake are the major N loss and sink. Export via discharge only occupies a small fraction.

The soil N leaching process was represented using a lumped reaction that generates  $\text{NO}_3^-$ . Conceptually this could represent the total rates of reactions including the decomposition of soil organic matter (SOM), nitrification, and rock weathering that generates  $\text{NO}_3^-$ . Its rate was assumed to depend on soil temperature and moisture and follows the equation  $r_{leach} = kAf(T)f(S_w)$ , where  $r_{leach}$  [mol/s] is the leaching rate,  $k = 10^{-9.7}$  [mol/m<sup>2</sup>/s] is the leaching rate constant (Regnier and Steefel, 1999), and  $A$  [m<sup>2</sup>] is the surface area that represents the contact area between substrates and N transforming microbe, and  $f(T)$  and  $f(S_w)$  are soil temperature (Eqn. 8) and soil moisture (Eqn. 9) functions, respectively. The surface area was calculated based on SOM volume fraction [m<sup>3</sup>/m<sup>3</sup>], specific surface area (SSA, [m<sup>2</sup>/g]), substrate density [g/cm<sup>3</sup>], and element volume [m<sup>3</sup>]. Denitrification converts  $\text{NO}_3^-$  to  $\text{N}_2$  gas under anaerobic conditions. Here this process was modeled by the Monod rate law with DOC as the electron donor (Di Capua

et al., 2019),  $\text{NO}_3^-$  as the electron acceptor, and with an inhibition term  $f(O_2)$  (Eqn. S13).

The reaction rate:  $r_{\text{denitrification}} = kA \frac{C_{\text{DOC}}}{K_{m,\text{DOC}} + C_{\text{DOC}}} \frac{C_{\text{NO}_3^-}}{K_{m,\text{NO}_3^-} + C_{\text{NO}_3^-}} f(O_2)f(T)f(S_w)$ , where  $k = 10^{-10}$  [mol/m<sup>2</sup>/s] is the denitrification rate constant (Regnier and Steefel, 1999), half-saturation constants  $K_{m,\text{DOC}} = 15$  [ $\mu\text{M}$ ] and  $K_{m,\text{NO}_3^-} = 45$  [ $\mu\text{M}$ ] (Regnier and Steefel, 1999; Billen, 1977). For soil N leaching and denitrification, the SSA were respectively tuned as  $1.6 \times 10^{-6}$  and  $7.5 \times 10^{-5}$  [m<sup>2</sup>/g] to reproduce observed stream nitrate dynamics. The calibrated values were orders of magnitude lower than the lab measured SSA of natural materials (e.g., SOM, 0.6 ~ 2 m<sup>2</sup>/g) (Rutherford et al., 1992; Chiou et al., 1990). Such discrepancies between calibrated effective reactive surface area (i.e., solid-water contact area) and lab measured absolute surface area are consistent with other observations in literature (Li et al., 2014; Heidari et al., 2017). The uptake rate constant was calibrated by constraining the partitioning of N transformation flux between denitrification and plant uptake by the ratio of 1:5, a value estimated from field measurements of gaseous N outputs (3.53 kg-N/ha/yr) and plant N uptake (18.3 kg-N/ha/yr) (Weitzman and Kaye, 2018). The uptake rate constant in the deep zone (> 2 m in depth) was considered negligible (Weitzman and Kaye, 2018; Hasenmueller et al., 2017). Groundwater nitrate was initialized as 0.43 mg/L, the average of measured groundwater concentration during 2009 - 2010.

**Temporal nitrate dynamics.** Three cases were set up to understand and quantify the effects of different processes in determining nitrate dynamics (Figure 8a). The *transport-only* case (dashed line, *tran*) simulates nitrate input from precipitation (at  $1.4 \pm 0.96$  mg/L, based on the 2009 data of NADP PA42 site) and N transport but without any reactions. It overestimated stream nitrate data ( $0.33 \pm 0.39$  mg/L) throughout the year. The *transport + N reactions* case (gray line, *tran + N react*) has denitrification and soil N leaching processes but not plant uptake. These two reactions lowered the nitrate concentration slightly, as these two processes compensate each other in adding and removing nitrate from water. The *transport + N reactions + uptake* case (thick black line, *tran + N react + upta*) have all processes. It significantly lowered the nitrate concentration, especially in April-May and October-December. Nitrate peaks from May to July, exhibiting comparable



levels of high precipitation nitrate concentration (Figure 8b). It is noticeable that the three cases almost overlapped at these overestimated short nitrate peaks, suggesting nitrate-rich precipitation may not be routed into the subsurface where denitrification and plant uptake could occur.

Although precipitation from April to August accounted for 70% of the total simulation period, larger storm events in October contributed more to the export. Deeper groundwater had higher nitrate concentration than shallow water, because most plant uptake occurred in the shallow zone. The nitrate fluxes into the deeper zone however only contributed 26% of stream nitrate export at the annual scale, due to the relatively small groundwater contribution (9.5%) to the stream. Denitrification and plant uptake largely occurred during the wet spring period, which is part of the leaf-on season. Denitrification peaks often appeared after major storm events. Comparing the three outfluxes (Figure 8c), nitrate export via discharge (red) was negligible compared to denitrification (blue) and plant uptake (green). At the annual scale, stream export only accounted for 9.5% outfluxes, whereas denitrification and plant uptake took up 15% and 75% of deposited  $\text{NO}_3^-$ , respectively. In other words, as Nitrate enters this system via precipitation, plant uptake can play a significant role in reducing nitrate level, indicating precipitated nitrate is tightly cycled in the system.

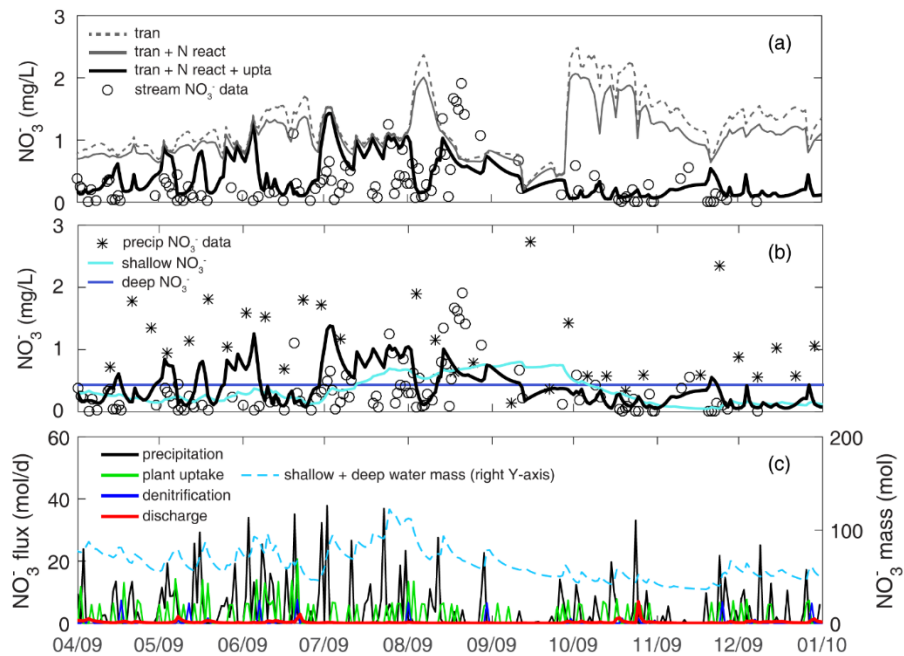


**Figure 8.** Stream nitrate dynamics and fluxes at Shale Hills in Example 2. (a) stream nitrate dynamics in three simulation conditions with different processes: *transport-only* (dashed line, *tran*), *transport + N reaction* (gray line, *tran + N react*), *transport + N reaction + plant uptake* (thick black line, *tran + N react + upta*), where N reactions include both nitrate leaching and denitrification (see Figure 7); (b) nitrate concentration in precipitation, shallow and deep water; (c) nitrate fluxes and budget. Note the nitrate leaching was ignored in (b) due to its minimal flux as precipitation N deposition was as the dominant input source (Weitzman and Kaye, 2018).

### 6.3 Example 3: DOC production and export in a spatially distributed domain

This example showcases the application of BioRT-Flux-PIHM in a spatially distributed mode. This work has been documented with full details in Wen et al. (2020). Here we only introduce some key features and capabilities in the spatially distributed mode. The Shale Hills catchment was discretized into 535 prismatic land elements and 20 stream segments through PIHMgis based on the topography (Figure 9a). The heterogeneous distributions of soil depth and solid organic carbon within the domain (Figure 9b-c) were interpolated through ordinary kriging based on field surveys (Andrews et al., 2011; Lin, 2006). Other soil and mineralogy properties such as hydraulic conductivity, van Genuchten parameters, and ion exchange capacity were spatially distributed following intensive field measurements (Jin and Brantley, 2011; Jin et al., 2010; Shi et al., 2013) ([criticalzone.org/shale-hills/data/](https://criticalzone.org/shale-hills/data/)).

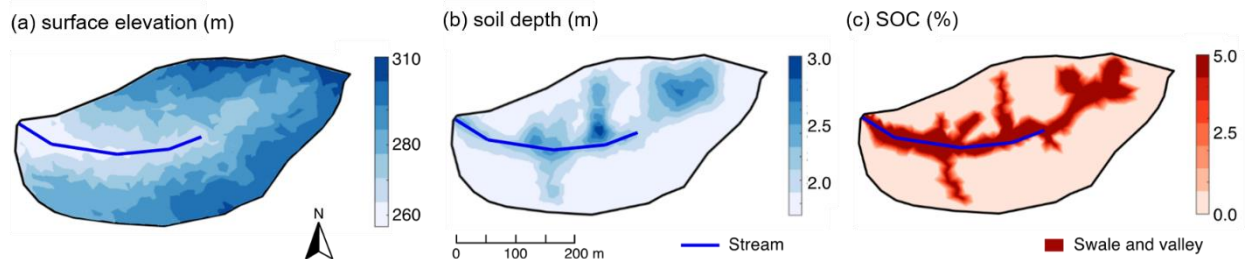


**Figure 9.** Attributes of Shale Hills in the spatially distributed mode in Example 3: (a) surface elevation, (b) soil depth, and (c) soil organic carbon (SOC). The surface elevation was generated from lidar topographic data ([criticalzone.org/shale-hills/data/](https://criticalzone.org/shale-hills/data/)); Soil depths and SOC were interpolated using ordinary kriging based on field surveys (Andrews et al., 2011; Lin, 2006). The SOC distribution in (c) was further simplified using the high, uniform SOC (5% v/v) in swales and valley soils based on field survey (Andrews et al., 2011). Swales and valley floor areas were defined based on surface elevation via field survey and a 10 m resolution digital elevation model (Lin, 2006).

**Temporal and spatial patterns of DOC production and export.** The model outputs followed the general trend of stream DOC measurements (NSE = 0.55 for monthly DOC concentration; Figure 10a), with high values (~15 mg/L) in the dry periods (July-September). The model enabled the identification of spatial patterns and hot spots of reactions. In May when soil water is relatively abundant, the valley and swales with deeper soils (Figure 10b) generally tended to be wetter compared to the hillslope and ridgetop, and were hydrologically connected to the stream (Figure 10b, c). The distribution of local DOC production rate  $r_{DOC}$  and DOC concentration followed that of SOC (Figure 10c) and water content (Figure 10b). Low  $r_{DOC}$  in relatively dry planar hillslopes and uplands resulted in low soil water DOC. The average stream DOC (~5 mg/L) reflected soil water DOC in the valley and swales.

In August, the hydrologically-connected zones with high water content shrank to the vicinity of the stream and river bed. With high temperature in summer,  $r_{DOC}$  increased by 2-fold from May across the whole catchment while still exhibited the highest values in the SOC-rich regions. Soil water DOC concentration increased by a factor of 2 because the produced DOC was trapped in low soil moisture areas that were not hydrologically connected to the stream. In the north side with low water content (Figure 10b), the soil water DOC (~7 mg/L in average) accumulated more than the south side (~5 mg/L in average). The high shallow water DOC (~10 mg/L) in the stream vicinity dominated the stream DOC in August.

In October, precipitation wetted the catchment again. The hydrologically connected zones expanded beyond swales and the valley to the upland hillslopes (Figure 10c). The increase in hydrological connectivity zones favored the mixing of shallow water DOC sourced from upland hillslopes (low DOC), swales, and valley (high DOC) into stream rather than only from the stream vicinity with high DOC in the dry August, leading to a drop in stream DOC.

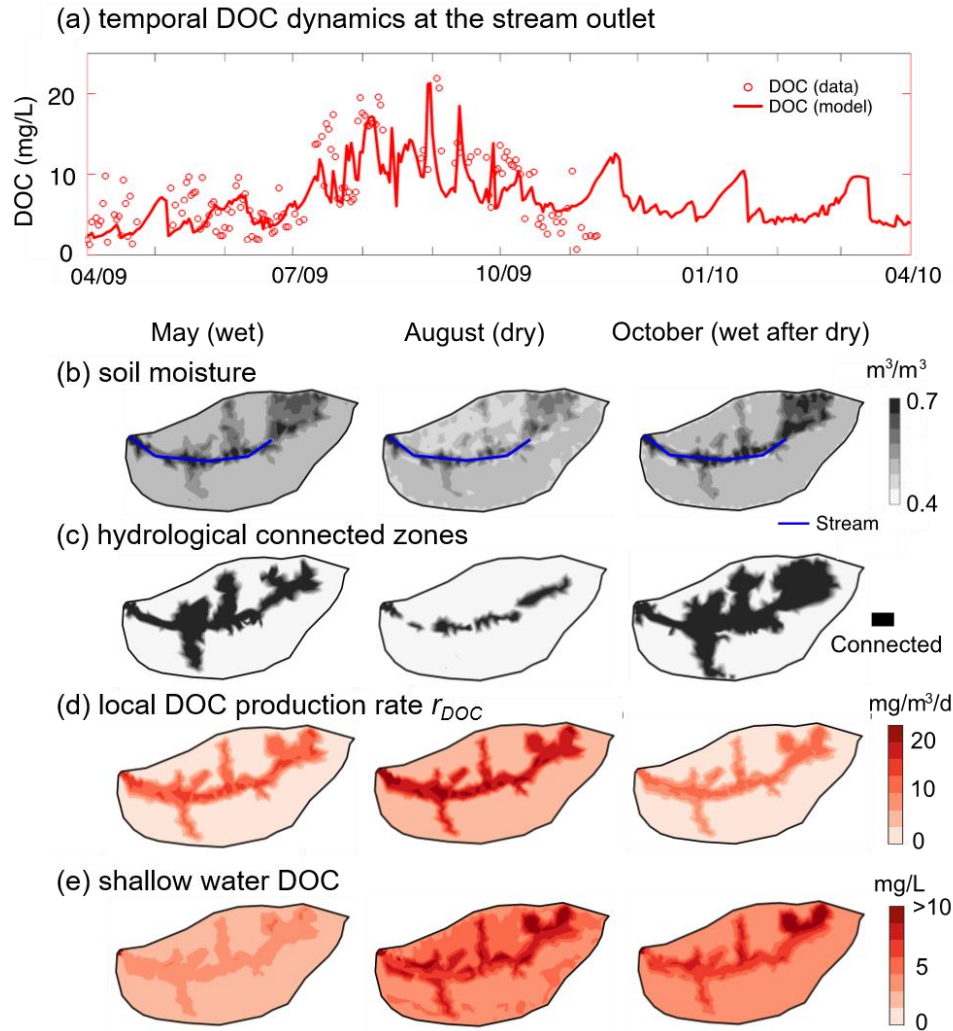


**Figure 10.** (a) Temporal dynamics of stream DOC concentration; spatial profiles of (b) shallow soil moisture, (c) hydrologically connected zones, (d) local DOC production rates  $r_{DOC}$  and (e) shallow water DOC concentration in May (wet), August (dry), and October (wet after dry) of 2009. The soil DOC and  $r_{DOC}$  were high in swales and valley with relatively high shallow water and SOC content. August had the highest shallow water DOC concentration compared to May and October, because most DOC accumulated in zones that are disconnected to the stream.

**C-Q patterns.** The DOC C-Q relationship showed a non-typical pattern with flushing first and transitioning into a dilution pattern, with an overall C-Q slope  $b = -0.23$  (Figure 11). At low discharges ( $< 1.8 \times 10^{-4}$  m/d) in the summer dry period, the stream DOC mainly came from the organic-rich swales and valley floor zones with high soil water DOC (Figure 10e). With discharge increasing in wetter period (i.e., spring and fall), the contribution

from planar hillslopes and uplands with lower DOC concentration increased (Figure 10e), leading to the dilution of stream DOC.

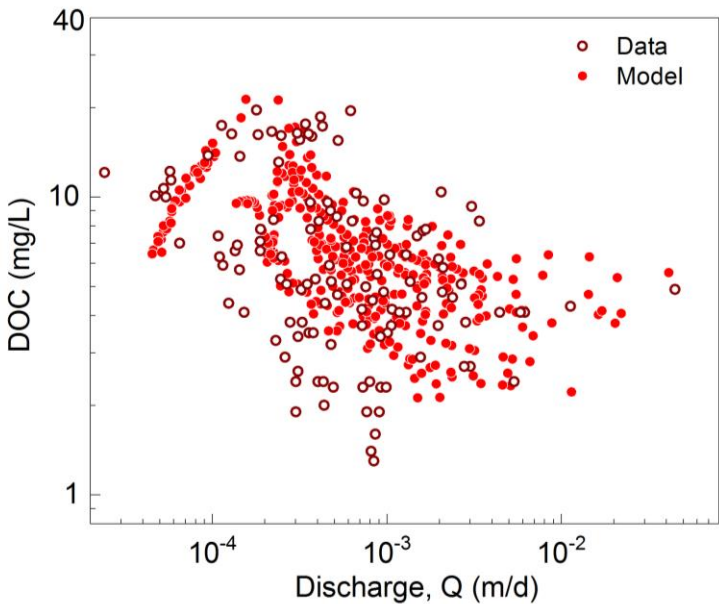


**Figure 11.** Relationships of daily discharge ( $Q$ ) with stream DOC concentration. With the increase of  $Q$ , the stream water first shifted from the dominance of groundwater with low DOC at very low discharge to the predominance of organic-rich soil water from swales and valley at intermediate discharge. As the discharge increases further, the stream water switches to the dominance of high flow with lower DOC water from planar hillslopes and uplands, resulting in a dilution C-Q pattern (modified from Wen et al., 2020).

## 7. Discussion

The watershed biogeochemical model BioRT-Flux-PIHM brings the reactive transport modeling capabilities to the watershed scale, enabling the simulation of subsurface shallow and deep flow paths and biogeochemical reactions influenced by hydroclimatic conditions and land-surface interactions. The expanded model capability of simulating bio-mediated processes such as plant uptake, soil respiration, and microbe-mediated redox reactions enables the simulation of carbon and nutrient cycling in the shallow subsurface. The inclusion of the deep groundwater zone allows the exploration of the effects of subsurface structure on hydrological partitioning between shallow soil lateral flow and deep groundwater, and their relationships with stream discharge. Although not shown here, the model can also simulate deeper groundwater coming from regional aquifers across the outer boundary. This can be particularly useful for

watersheds of higher stream orders, where a large proportion of deep water may come from nearby regional aquifers.

The model presented here is complex and process-based. The computational cost of solving a spatially distributed, nonlinear, multi-component reactive transport model is high, posing challenges for the application of ensemble-based uncertainty analysis and model weighting/selection methods (Song et al., 2015). With additional reaction and transport processes, the model includes more functions (such as reaction kinetic rate laws) and parameters (e.g., reaction rate constants, surface area) than hydrological models, which have already been criticized for their complexity, equifinality, uncertainty, and data demands (Beven, 2001, 2006;Kirchner et al., 1996). These issues will persist even though reactive transport models will be constrained by additional chemical data. A major source of uncertainty in these models lies in epistemic uncertainties, i.e., the lack of specific knowledge in forcing data and details of reactivities (e.g., spatial distribution and abundance of reactive materials), on top of uncertainties related to hydrology (Beven, 2000;Beven and Freer, 2001). The model's conceptual foundations also represent a major source of uncertainty.

It is in this spirit of “balancing” the cost and gain that we present both spatial distributed and lumped modes for the BioRT model. Compared to the distributed version, the spatially implicit model requires less spatial data, is computationally inexpensive, and is relatively easy to set up. It can assess the average dynamics of the water and solute dynamics and focus on the interactions among processes without resolving spatial details. The lumped approach can also accommodate basins with low data availability, and it can be easier for students to learn to use the model. In contrast, spatially explicit representations enable the exploration of the “hot spots” (e.g., swales and riparian zones with high soil water DOC concentrations in Figure 10e) and their contribution to stream chemistry at different times. Spatial heterogeneities in watershed properties (e.g., soil types and depth, lithology, vegetation, biomass, and mineralogy) are ubiquitous in natural systems. However, a general understanding of the linkage between local catchment features and catchment-scale dynamics (e.g., stream concentration dynamics and solute export pattern) is often lacking. We generally do not understand how spatial heterogeneity affects water flow paths, stream water chemistry, and biogeochemical reaction rates. The

spatially distributed model provides a tool to further explore these questions. Ultimately, the choice of the model complexity level depends on the research questions that the model is set to answer. At the end, we all need to balance cost and gain when deciding to use a simple or complex model, striving to be “simple but not simplistic” (Beven and Lane, 2019).

## **8. Summary and conclusion**

This paper introduces the watershed-scale biogeochemical reactive transport code BioRT (short for BioRT-Flux-PIHM). The code integrates processes of land-surface interactions, surface hydrology, and multi-component biogeochemical reactive transport. The new development enables the simulation of 1) biotic reactions including plant uptake, soil respiration, and microbe-mediated redox reactions, and 2) surface water interactions with groundwater from deeper subsurface that still interacts with streams. BioRT has been verified against the widely used reactive transport code CrunchTope for soil carbon, nitrogen, and phosphorus processes. The BioRT module has been applied to understand carbon, nitrogen, and weathering processes in Shale Hills in Pennsylvania, Coal Creek in Colorado, and Volcán Chimborazo watershed in Andes in Ecuador. Here we showcase the modeling capability of surface-groundwater interactions and reactive transport processes relevant to nitrate and DOC in Shale Hills in two simulation modes. One is in a spatially lumped mode using averaged properties and another is in a spatially distributed mode with consideration of spatial heterogeneity. Results show that the deep groundwater flow that interacts with the stream is primarily controlled by the hydraulic conductivity contrast between shallow and deep zone. biogeochemical reactions in shallow soil primarily determine the stream water chemistry under high flow conditions. The spatially lumped method with two lumped grids can capture the temporal dynamics of average behavior and mass balance; the spatially distributed running mode can be used to understand the spatial dynamics and to identify “hot spots” of reactions. The code can be used for biogeochemical reactive transport simulations in watersheds under diverse climate, land cover, and geology conditions.



**Data availability.** Field data (e.g., discharge, stream chemistry) is archived at Shale Hills data portal: <http://criticalzone.org/shale-hills/data/datasets/> or maintained at HydroShare: <https://www.hydroshare.org/group/147>.

**Code availability.** The current model release (BioRT-Flux-PIHM v1.0), including documentation, source code, example data, is available at GitHub repository: <https://github.com/PSUmodeling/BioRT-Flux-PIHM>.

**Competing interests.** The authors declare that they have no conflict of interest.

**Author contributions.** LL conceived the model idea and oversaw the model development. WZ coded the BioRT module, verified the code against the benchmark reactive transport model CrunchTope, and applied and tested the model at Shale Hills watershed. YS developed the deep groundwater component and integrated the BioRT-Flux-PIHM v1.0 into the MM-PIHM family. WH, LS, KS, DK, BS, and GHCH tested the code during its development and contributed study cases.

**Acknowledgement.** We acknowledge the funding support from the Department of Energy, Subsurface Biogeochemistry Program DE-SC0020146, National Science Foundation Hydrological Sciences EAR-1758795. LS and GCN were supported by National Science Foundation Grant EAR-1759071. We appreciate data from the Susquehanna Shale Hills Critical Zone Observatory (SSHCZO) supported by National Science Foundation Grant EAR – 0725019 (C. Duffy), EAR – 1239285 (S. Brantley), and EAR – 1331726 (S. Brantley). Data were collected in Penn State's Stone Valley Forest, which is funded by the Penn State College of Agriculture Sciences, Department of Ecosystem Science and Management, and managed by the staff of the Forestlands Management Office.



## 809    **References**

- 810    Andrews, D. M., Lin, H., Zhu, Q., Jin, L., and Brantley, S. L.: Hot spots and hot moments of dissolved organic  
811    carbon export and soil organic carbon storage in the Shale Hills catchment, *Vadose Zone Journal*, 10, 943-  
812    954, 2011.
- 813    Anyah, R. O., Weaver, C. P., Miguez - Macho, G., Fan, Y., and Robock, A.: Incorporating water table  
814    dynamics in climate modeling: 3. Simulated groundwater influence on coupled land - atmosphere  
815    variability, *Journal of Geophysical Research: Atmospheres*, 113, 2008.
- 816    Bai, J., Zhang, G., Zhao, Q., Lu, Q., Jia, J., Cui, B., and Liu, X.: Depth-distribution patterns and control of soil  
817    organic carbon in coastal salt marshes with different plant covers, *Sci Rep-Uk*, 6, 34835,  
818    10.1038/srep34835, 2016.
- 819    Bailey, R., Rathjens, H., Bieger, K., Chaubey, I., and Arnold, J.: SWATMOD-Prep: Graphical User Interface  
820    for Preparing Coupled SWAT-MODFLOW Simulations, *JAWRA Journal of the American Water Resources*  
821    Association, 53, 400-410, <https://doi.org/10.1111/1752-1688.12502>, 2017.
- 822    Bao, C., Wu, H., Li, L., Newcomer, D., Long, P. E., and Williams, K. H.: Uranium Bioreduction Rates across  
823    Scales: Biogeochemical Hot Moments and Hot Spots during a Biostimulation Experiment at Rifle, Colorado,  
824    *Environmental Science & Technology*, 48, 10116-10127, 10.1021/es501060d, 2014.
- 825    Bao, C., Li, L., Shi, Y., and Duffy, C.: Understanding watershed hydrogeochemistry: 1. Development of RT -  
826    Flux - PIHM, *Water Resources Research*, 53, 2328-2345, 2017.
- 827    Basu, N. B., Destouni, G., Jawitz, J. W., Thompson, S. E., Loukinova, N. V., Darracq, A., Zanardo, S., Yaeger,  
828    M., Sivapalan, M., Rinaldo, A., and Rao, P. S. C.: Nutrient loads exported from managed catchments reveal  
829    emergent biogeochemical stationarity, *Geophys. Res. Lett.*, 37, 10.1029/2010GL045168, 2010.
- 830    Beven, K.: How far can we go in distributed hydrological modelling?, *Hydrol. Earth Syst. Sci.*, 5, 1-12,  
831    10.5194/hess-5-1-2001, 2001.
- 832    Beven, K., and Freer, J.: Equifinality, data assimilation, and uncertainty estimation in mechanistic  
833    modelling of complex environmental systems using the GLUE methodology, *Journal of Hydrology*, 249,  
834    11-29, 10.1016/S0022-1694(01)00421-8, 2001.
- 835    Beven, K.: A manifesto for the equifinality thesis, *Journal of Hydrology*, 320, 18-36,  
836    10.1016/j.jhydrol.2005.07.007, 2006.
- 837    Beven, K., and Lane, S.: Invalidation of Models and Fitness-for-Purpose: A Rejectionist Approach, in:  
838    *Computer Simulation Validation: Fundamental Concepts, Methodological Frameworks, and Philosophical*  
839    *Perspectives*, edited by: Beisbart, C., and Saam, N. J., Springer International Publishing, Cham, 145-171,  
840    2019.
- 841    Beven, K. J.: Uniqueness of place and process representations in hydrological modelling, *Hydrol. Earth*  
842    *Syst. Sci.*, 4, 203-213, 10.5194/hess-4-203-2000, 2000.
- 843    Bhatt, G., Kumar, M., and Duffy, C. J.: A tightly coupled GIS and distributed hydrologic modeling  
844    framework, *Environmental Modelling & Software*, 62, 70-84,  
845    <http://dx.doi.org/10.1016/j.envsoft.2014.08.003>, 2014.
- 846    Billen, G.: *Etude écologique des transformations de l'azote dans les sédiments marins*, 1977.
- 847    Bracho, R., Natali, S., Pegoraro, E., Crummer, K. G., Schädel, C., Celis, G., Hale, L., Wu, L., Yin, H., and Tiedje,  
848    J. M.: Temperature sensitivity of organic matter decomposition of permafrost-region soils during  
849    laboratory incubations, *Soil Biology and Biochemistry*, 97, 1-14, 2016.
- 850    Brantley, S. L., Kubicki, J. D., and White, A. F.: Kinetics of water-rock interaction, 2008.
- 851    Brantley, S. L., White, T., West, N., Williams, J. Z., Forsythe, B., Shapich, D., Kaye, J., Lin, H., Shi, Y. N., Kaye,  
852    M., Herndon, E., Davis, K. J., He, Y., Eissenstat, D., Weitzman, J., DiBiase, R., Li, L., Reed, W., Brubaker, K.,  
853    and Gu, X.: Susquehanna Shale Hills Critical Zone Observatory: Shale Hills in the Context of Shaver's Creek  
854    Watershed, *Vadose Zone Journal*, 17, 1-19, ARTN 180092

10.2136/vzj2018.04.0092, 2018.

Brooks, P. D., Chorover, J., Fan, Y., Godsey, S. E., Maxwell, R. M., McNamara, J. P., and Tague, C.: Hydrological partitioning in the critical zone: Recent advances and opportunities for developing transferable understanding of water cycle dynamics, *Water Resources Research*, 51, 6973-6987, <https://doi.org/10.1002/2015WR017039>, 2015.

Buljovic, Z., and Engels, C.: Nitrate uptake ability by maize roots during and after drought stress, *Plant and Soil*, 229, 125-135, 2001.

Buyse, J., Smolders, E., and Merckx, R.: Modelling the uptake of nitrate by a growing plant with an adjustable root nitrate uptake capacity, *Plant and Soil*, 181, 19-23, 1996.

Cai, X., Yang, Z.-L., Fisher, J., Zhang, X., Barlage, M., and Chen, F.: Integration of nitrogen dynamics into the Noah-MP land surface model v1. 1 for climate and environmental predictions, *Geoscientific Model Development* (Online), 9, 2016.

Chiou, C. T., Lee, J. F., and Boyd, S. A.: The surface area of soil organic matter, *Environmental Science & Technology*, 24, 1164-1166, 1990.

Condon, L. E., Maxwell, R. M., and Gangopadhyay, S.: The impact of subsurface conceptualization on land energy fluxes, *Advances in Water Resources*, 60, 188-203, <https://doi.org/10.1016/j.advwatres.2013.08.001>, 2013.

Crawford, N. M., and Glass, A. D.: Molecular and physiological aspects of nitrate uptake in plants, *Trends in plant science*, 3, 389-395, 1998.

Davidson, E. A., and Janssens, I. A.: Temperature sensitivity of soil carbon decomposition and feedbacks to climate change, *Nature*, 440, 165-173, [10.1038/nature04514](https://doi.org/10.1038/nature04514), 2006.

Davidson, E. A., Janssens, I. A., and Luo, Y.: On the variability of respiration in terrestrial ecosystems: moving beyond Q10, *Global Change Biology*, 12, 154-164, 2006.

Davidson, E. A., Janssens, I.A.: Temperature sensitivity of soil carbon decomposition and feedbacks to climate change, *Nature*, 440, 165-173, 2006.

Devienne-Barret, F., Justes, E., Machet, J., and Mary, B.: Integrated control of nitrate uptake by crop growth rate and soil nitrate availability under field conditions, *Annals of Botany*, 86, 995-1005, 2000.

Di Capua, F., Pirozzi, F., Lens, P. N. L., and Esposito, G.: Electron donors for autotrophic denitrification, *Chemical Engineering Journal*, 362, 922-937, <https://doi.org/10.1016/j.cej.2019.01.069>, 2019.

Dingman, S. L.: *Physical hydrology*, Waveland press, 2015.

Dunbabin, V. M., Diggle, A. J., Rengel, Z., and Van Hugten, R.: Modelling the interactions between water and nutrient uptake and root growth, *Plant and Soil*, 239, 19-38, 2002.

Edwards, P. J., Williard, K. W. J., and Schoonover, J. E.: Fundamentals of Watershed Hydrology, *Journal of Contemporary Water Research & Education*, 154, 3-20, [10.1111/j.1936-704X.2015.03185.x](https://doi.org/10.1111/j.1936-704X.2015.03185.x), 2015.

Fatichi, S., Vivoni, E. R., Ogden, F. L., Ivanov, V. Y., Mirus, B., Gochis, D., Downer, C. W., Camporese, M., Davison, J. H., Ebel, B., Jones, N., Kim, J., Mascaro, G., Niswonger, R., Restrepo, P., Rigon, R., Shen, C., Sulis, M., and Tarboton, D.: An overview of current applications, challenges, and future trends in distributed process-based models in hydrology, *Journal of Hydrology*, 537, 45-60, <https://doi.org/10.1016/j.jhydrol.2016.03.026>, 2016.

Fatichi, S., Manzoni, S., Or, D., and Paschalis, A.: A Mechanistic Model of Microbially Mediated Soil Biogeochemical Processes: A Reality Check, *Global Biogeochemical Cycles*, 33, 620-648, [10.1029/2018gb006077](https://doi.org/10.1029/2018gb006077), 2019.

Fisher, J., Sitch, S., Malhi, Y., Fisher, R., Huntingford, C., and Tan, S. Y.: Carbon cost of plant nitrogen acquisition: A mechanistic, globally applicable model of plant nitrogen uptake, retranslocation, and fixation, *Global Biogeochemical Cycles*, 24, 2010.

Friedlingstein, P., Cox, P., Betts, R., Bopp, L., von Bloh, W., Brovkin, V., Cadule, P., Doney, S., Eby, M., and Fung, I.: Climate-carbon cycle feedback analysis: results from the C4MIP model intercomparison, *Journal of climate*, 19, 3337-3353, 2006.

903 Gassman, P. W., Reyes, M. R., Green, C. H., and Arnold, J. G.: The soil and water assessment tool: Historical  
 904 development, applications, and future research directions, *T Asabe*, 50, 1211-1250, 2007.  
 905 Gatel, L., Lauvernet, C., Carluer, N., Weill, S., Tournebize, J., and Paniconi, C.: Global evaluation and  
 906 sensitivity analysis of a physically based flow and reactive transport model on a laboratory experiment,  
 907 *Environmental Modelling & Software*, 113, 73-83, <https://doi.org/10.1016/j.envsoft.2018.12.006>, 2019.  
 908 Gleeson, T., Befus, K. M., Jasechko, S., Luijendijk, E., and Cardenas, M. B.: The global volume and  
 909 distribution of modern groundwater, *Nature Geoscience*, 9, 161, [10.1038/ngeo2590](https://doi.org/10.1038/ngeo2590)  
 910 <https://www.nature.com/articles/ngeo2590#supplementary-information>, 2015.  
 911 Godsey, S. E., Kirchner, J. W., and Clow, D. W.: Concentration–discharge relationships reflect chemostatic  
 912 characteristics of US catchments, *Hydrol. Process.*, 23, 1844-1864, [10.1002/hyp.7315](https://doi.org/10.1002/hyp.7315), 2009.  
 913 Godsey, S. E., Hartmann, J., and Kirchner, J. W.: Catchment chemostasis revisited: Water quality responds  
 914 differently to variations in weather and climate, *Hydrological Processes*, 33, 3056-3069,  
 915 <https://doi.org/10.1002/hyp.13554>, 2019.  
 916 Grathwohl, P., Rügner, H., Wöhling, T., Osenbrück, K., Schwientek, M., Gayler, S., Wollschläger, U., Selle,  
 917 B., Pause, M., and Delfs, J.-O.: Catchments as reactors: a comprehensive approach for water fluxes and  
 918 solute turnover, *Environmental earth sciences*, 69, 317-333, 2013.  
 919 Green, T. R.: Linking climate change and groundwater, in: *Integrated groundwater management*, Springer,  
 920 Cham, 97-141, 2016.  
 921 Gurdak, J. J.: Groundwater: Climate-induced pumping, *Nature Geoscience*, 10, 71, 2017.  
 922 Hachiya, T., and Sakakibara, H.: Interactions between nitrate and ammonium in their uptake, allocation,  
 923 assimilation, and signaling in plants, *Journal of Experimental Botany*, 68, 2501-2512, [10.1093/jxb/erw449](https://doi.org/10.1093/jxb/erw449),  
 924 2016.  
 925 Hamamoto, S., Moldrup, P., Kawamoto, K., and Komatsu, T.: Excluded - volume expansion of Archie's law  
 926 for gas and solute diffusivities and electrical and thermal conductivities in variably saturated porous  
 927 media, *Water Resources Research*, 46, 2010.  
 928 Han, B., Benner, S. G., and Flores, A. N.: Including Variability across Climate Change Projections in  
 929 Assessing Impacts on Water Resources in an Intensively Managed Landscape, *Water*, 11, 286, 2019.  
 930 Hararuk, O., Smith, M. J., and Luo, Y.: Microbial models with data-driven parameters predict stronger soil  
 931 carbon responses to climate change, *Glob. Chang. Biol.*, 21, 2439-2453, [10.1111/gcb.12827](https://doi.org/10.1111/gcb.12827), 2015.  
 932 HARTLEY, I. P., HEINEMEYER, A., and INESON, P.: Effects of three years of soil warming and shading on the  
 933 rate of soil respiration: substrate availability and not thermal acclimation mediates observed response,  
 934 *Global Change Biology*, 13, 1761-1770, <https://doi.org/10.1111/j.1365-2486.2007.01373.x>, 2007.  
 935 Hartmann, J., Lauerwald, R., and Moosdorf, N.: A brief overview of the GLObal River CHEmistry Database,  
 936 *GLORICH, Procedia Earth and Planetary Science*, 10, 23-27, 2014.  
 937 Hasenmueller, E. A., Jin, L., Stinchcomb, G. E., Lin, H., Brantley, S. L., and Kaye, J. P.: Topographic controls  
 938 on the depth distribution of soil CO<sub>2</sub> in a small temperate watershed, *Applied Geochemistry*, 63, 58-69,  
 939 2015.  
 940 Hasenmueller, E. A., Gu, X., Weitzman, J. N., Adams, T. S., Stinchcomb, G. E., Eissenstat, D. M., Drohan, P.  
 941 J., Brantley, S. L., and Kaye, J. P.: Weathering of rock to regolith: The activity of deep roots in bedrock  
 942 fractures, *Geoderma*, 300, 11-31, 2017.  
 943 Heidari, P., Li, L., Jin, L., Williams, J. Z., and Brantley, S. L.: A reactive transport model for Marcellus shale  
 944 weathering, *Geochimica et Cosmochimica Acta*, 217, 421-440, 2017.  
 945 Herndon, E. M., Dere, A. L., Sullivan, P. L., Norris, D., Reynolds, B., and Brantley, S. L.: Landscape  
 946 heterogeneity drives contrasting concentration–discharge relationships in shale headwater catchments,  
 947 *Hydrology and earth system sciences*, 19, 3333-3347, 2015.

948 Hindmarsh, A. C., Brown, P. N., Grant, K. E., Lee, S. L., Serban, R., Shumaker, D. E., and Woodward, C. S.:  
 949 SUNDIALS: Suite of nonlinear and differential/algebraic equation solvers, *ACM Transactions on*  
 950 *Mathematical Software (TOMS)*, 31, 363-396, 2005.  
 951 Hodges, C., Kim, H., Brantley, S. L., and Kaye, J.: Soil CO<sub>2</sub> and O<sub>2</sub> Concentrations Illuminate the Relative  
 952 Importance of Weathering and Respiration to Seasonal Soil Gas Fluctuations, *Soil Science Society of*  
 953 *America Journal*, 83, 1167-1180, 2019.  
 954 Hubbard, S. S., Williams, K. H., Agarwal, D., Banfield, J., Beller, H., Bouskill, N., Brodie, E., Carroll, R.,  
 955 Dafflon, B., and Dwivedi, D.: The East River, Colorado, Watershed: A mountainous community testbed for  
 956 improving predictive understanding of multiscale hydrological–biogeochemical dynamics, *Vadose Zone*  
 957 *Journal*, 17, 2018.  
 958 Husic, A.: Numerical modeling and isotope tracers to investigate karst biogeochemistry and transport  
 959 processes, 2018.  
 960 Jin, L., and Brantley, S. L.: Soil chemistry and shale weathering on a hillslope influenced by convergent  
 961 hydrologic flow regime at the Susquehanna/Shale Hills Critical Zone Observatory, *Applied Geochemistry*,  
 962 26, Supplement, S51-S56, <http://dx.doi.org/10.1016/j.apgeochem.2011.03.027>, 2011.  
 963 Jin, L. X., Ravella, R., Ketchum, B., Bierman, P. R., Heaney, P., White, T., and Brantley, S. L.: Mineral  
 964 weathering and elemental transport during hillslope evolution at the Susquehanna/Shale Hills Critical  
 965 Zone Observatory, *Geochim Cosmochim Acta*, 74, 3669-3691, 10.1016/j.gca.2010.03.036, 2010.  
 966 Keune, J., Gasper, F., Goergen, K., Hense, A., Shrestha, P., Sulis, M., and Kollet, S.: Studying the influence  
 967 of groundwater representations on land surface-atmosphere feedbacks during the European heat wave  
 968 in 2003, *Journal of Geophysical Research: Atmospheres*, 121, 13,301-313,325,  
 969 <https://doi.org/10.1002/2016JD025426>, 2016.  
 970 Kirchner, J. W., Hooper, R. P., Kendall, C., Neal, C., and Leavesley, G.: Testing and validating environmental  
 971 models, *Science of the Total Environment*, 183, 33-47, 10.1016/0048-9697(95)04971-1, 1996.  
 972 Kirchner, J. W.: A double paradox in catchment hydrology and geochemistry, *Hydrol. Process.*, 17, 871-  
 973 874, 10.1002/hyp.5108, 2003.  
 974 Kuntz, B. W., Rubin, S., Berkowitz, B., and Singha, K.: Quantifying Solute Transport at the Shale Hills Critical  
 975 Zone Observatory, *Vadose Zone Journal*, 10, 843-857, 10.2136/vzj2010.0130, 2011.  
 976 Lam, Q. D., Schmalz, B., and Fohrer, N.: Modelling point and diffuse source pollution of nitrate in a rural  
 977 lowland catchment using the SWAT model, *Agricultural Water Management*, 97, 317-325,  
 978 <https://doi.org/10.1016/j.agwat.2009.10.004>, 2010.  
 979 Leonard, L., and Duffy, C. J.: Essential terrestrial variable data workflows for distributed water resources  
 980 modeling, *Environmental modelling & software*, 50, 85-96, 2013.  
 981 Li, L., Salehikhoo, F., Brantley, S. L., and Heidari, P.: Spatial zonation limits magnesite dissolution in porous  
 982 media, *Geochimica et Cosmochimica Acta*, 126, 555-573, 10.1016/j.gca.2013.10.051, 2014.  
 983 Li, L., Bao, C., Sullivan, P. L., Brantley, S., Shi, Y., and Duffy, C.: Understanding watershed  
 984 hydrogeochemistry: 2. Synchronized hydrological and geochemical processes drive stream chemostatic  
 985 behavior, *Water Resources Research*, 53, 2346-2367, 2017a.  
 986 Li, L., Maher, K., Navarre-Sitchler, A., Druhan, J., Meile, C., Lawrence, C., Moore, J., Perdrial, J., Sullivan, P.,  
 987 Thompson, A., Jin, L., Bolton, E. W., Brantley, S. L., Dietrich, W. E., Mayer, K. U., Steefel, C. I., Valocchi, A.,  
 988 Zachara, J., Kocar, B., McIntosh, J., Tutolo, B. M., Kumar, M., Sonnenthal, E., Bao, C., and Beisman, J.:  
 989 Expanding the role of reactive transport models in critical zone processes, *Earth-Science Reviews*, 165,  
 990 280-301, <http://dx.doi.org/10.1016/j.earscirev.2016.09.001>, 2017b.  
 991 Li, L.: Watershed reactive transport, *Reviews in Mineralogy and Geochemistry*, 85, 381-418, 2019.  
 992 Li, L., Sullivan, P. L., Benettin, P., Cirpka, O. A., Bishop, K., Brantley, S. L., Knapp, J. L. A., Meerveld, I.,  
 993 Rinaldo, A., Seibert, J., Wen, H., and Kirchner, J. W.: Toward catchment hydro - biogeochemical theories,  
 994 *WIREs Water*, 10.1002/wat2.1495, 2020.

995 Lin, H.: Temporal stability of soil moisture spatial pattern and subsurface preferential flow pathways in  
 996 the shale hills catchment, *Vadose Zone J*, 5, 317-340, 10.2136/vzj2005.0058, 2006.  
 997 Lindström, G., Rosberg, J., and Arheimer, B.: Parameter Precision in the HBV-NP Model and Impacts on  
 998 Nitrogen Scenario Simulations in the Rönneå River, Southern Sweden, *AMBIO: A Journal of the Human*  
 999 *Environment*, 34, 533-537, 535, 2005.  
 1000 Lindström, G., Pers, C., Rosberg, J., Strömqvist, J., and Arheimer, B.: Development and testing of the HYPE  
 1001 (Hydrological Predictions for the Environment) water quality model for different spatial scales, *Hydrology*  
 1002 *Research*, 41, 295-319, 10.2166/nh.2010.007, 2010.  
 1003 Liu, Y., Wang, C., He, N., Wen, X., Gao, Y., Li, S., Niu, S., Butterbach - Bahl, K., Luo, Y., and Yu, G.: A global  
 1004 synthesis of the rate and temperature sensitivity of soil nitrogen mineralization: latitudinal patterns and  
 1005 mechanisms, *Global change biology*, 23, 455-464, 2017.  
 1006 López, B., Sabaté, S., and Gracia, C.: Vertical distribution of fine root density, length density, area index  
 1007 and mean diameter in a *Quercus ilex* forest, *Tree Physiology*, 21, 555-560, 2001.  
 1008 Maavara, T., Lauerwald, R., Laruelle, G. G., Akbarzadeh, Z., Bouskill, N. J., Van Cappellen, P., and Regnier,  
 1009 P.: Nitrous oxide emissions from inland waters: Are IPCC estimates too high?, *Global Change Biology*, 0,  
 1010 doi:10.1111/gcb.14504, 2018.  
 1011 Martínez-de la Torre, A., and Miguez-Macho, G.: Groundwater influence on soil moisture memory and  
 1012 land-atmosphere fluxes in the Iberian Peninsula, *Hydrology and Earth System Sciences*, 23, 4909-4932,  
 1013 2019.  
 1014 Maxwell, R. M., Lundquist, J. K., Mirocha, J. D., Smith, S. G., Woodward, C. S., and Tompson, A. F.:  
 1015 Development of a coupled groundwater-atmosphere model, *Monthly Weather Review*, 139, 96-116,  
 1016 2011.  
 1017 Mayer, K. U., Frind, E. O., and Blowes, D. W.: Multicomponent reactive transport modeling in variably  
 1018 saturated porous media using a generalized formulation for kinetically controlled reactions, *Water*  
 1019 *Resources Research*, 38, 13-11-13-21, 10.1029/2001wr000862, 2002.  
 1020 McMurtrie, R. E., Iversen, C. M., Dewar, R. C., Medlyn, B. E., Näsholm, T., Pepper, D. A., and Norby, R. J.:  
 1021 Plant root distributions and nitrogen uptake predicted by a hypothesis of optimal root foraging, *Ecology*  
 1022 *and Evolution*, 2, 1235-1250, 2012.  
 1023 Miller, M. P., Tesoriero, A. J., Hood, K., Terziotti, S., and Wolock, D. M.: Estimating Discharge and Nonpoint  
 1024 Source Nitrate Loading to Streams From Three End-Member Pathways Using High-Frequency Water  
 1025 Quality Data, *Water Resources Research*, 53, 10201-10216, 10.1002/2017wr021654, 2017.  
 1026 Miller, M. P., Capel, P. D., García, A. M., and Ator, S. W.: Response of Nitrogen Loading to the Chesapeake  
 1027 Bay to Source Reduction and Land Use Change Scenarios: A SPARROW - Informed Analysis, *JAWRA*  
 1028 *Journal of the American Water Resources Association*, 56, 100-112, 2020.  
 1029 Moatar, F., Abbott, B. W., Minaudo, C., Curie, F., and Pinay, G.: Elemental properties, hydrology, and  
 1030 biology interact to shape concentration - discharge curves for carbon, nutrients, sediment, and major  
 1031 ions, *Water Resources Research*, 53, 1270-1287, 2017.  
 1032 Moriasi, D. N., Gowda, P. H., Arnold, J. G., Mulla, D. J., Ale, S., and Steiner, J. L.: Modeling the impact of  
 1033 nitrogen fertilizer application and tile drain configuration on nitrate leaching using SWAT, *Agricultural*  
 1034 *Water Management*, 130, 36-43, <https://doi.org/10.1016/j.agwat.2013.08.003>, 2013.  
 1035 Musolff, A., Schmidt, C., Selle, B., and Fleckenstein, J. H.: Catchment controls on solute export, *Adv. Water*  
 1036 *Resour.*, 86, 133-146, 10.1016/j.advwatres.2015.09.026, 2015.  
 1037 Neitsch, S. L., Arnold, J. G., Kiniry, J. R., and Williams, J. R.: Soil and water assessment tool theoretical  
 1038 documentation version 2009, Texas Water Resources Institute, 2011.  
 1039 Ottoy, S., Elsen, A., Van De Vreken, P., Gobin, A., Merckx, R., Hermy, M., and Van Orshoven, J.: An  
 1040 exponential change decline function to estimate soil organic carbon stocks and their changes from topsoil  
 1041 measurements, *European Journal of Soil Science*, 67, 816-826, 2016.

Porporato, A., D'odorico, P., Laio, F., and Rodriguez-Iturbe, I.: Hydrologic controls on soil carbon and nitrogen cycles. I. Modeling scheme, *Advances in water resources*, 26, 45-58, 2003.

Qu, Y., and Duffy, C. J.: A semidiscrete finite volume formulation for multiprocess watershed simulation, *Water Resources Research*, 43, W08419, 2007.

Ranalli, A. J., and Macalady, D. L.: The importance of the riparian zone and in-stream processes in nitrate attenuation in undisturbed and agricultural watersheds – A review of the scientific literature, *Journal of Hydrology*, 389, 406-415, <https://doi.org/10.1016/j.jhydrol.2010.05.045>, 2010.

Regnier, P., and Steefel, C. I.: A high resolution estimate of the inorganic nitrogen flux from the Scheldt estuary to the coastal North Sea during a nitrogen-limited algal bloom, spring 1995, *Geochimica et Cosmochimica Acta*, 63, 1359-1374, [10.1016/S0016-7037\(99\)00034-4](https://doi.org/10.1016/S0016-7037(99)00034-4), 1999.

Rutherford, D. W., Chiou, C. T., and Kile, D. E.: Influence of soil organic matter composition on the partition of organic compounds, *Environmental science & technology*, 26, 336-340, 1992.

Saad, Y., and Schultz, M. H.: GMRES: A generalized minimal residual algorithm for solving nonsymmetric linear systems, *SIAM Journal on scientific and statistical computing*, 7, 856-869, 1986.

Saberi, L., Ng, G.-H. C., Nelson, L., Zhi, W., Li, L., La Frenierre, J., and Johnstone, M.: Spatiotemporal Drivers of Hydrochemical Variability in a Tropical Glacierized Watershed in the Andes, under review.

Saha, D., Rau, B. M., Kaye, J. P., Montes, F., Adler, P. R., and Kemanian, A. R.: Landscape control of nitrous oxide emissions during the transition from conservation reserve program to perennial grasses for bioenergy, *GCB Bioenergy*, 9, 783-795, [doi:10.1111/gcbb.12395](https://doi.org/10.1111/gcbb.12395), 2017.

Scudeler, C., Pangle, L., Pasetto, D., Niu, G.-Y., Volkmann, T., Paniconi, C., Putti, M., and Troch, P.: Multiresponse modeling of variably saturated flow and isotope tracer transport for a hillslope experiment at the Landscape Evolution Observatory, *Hydrology and Earth System Sciences*, 20, 4061-4078, 2016.

Sebestyen, S. D., Ross, D. S., Shanley, J. B., Elliott, E. M., Kendall, C., Campbell, J. L., Dail, D. B., Fernandez, I. J., Goodale, C. L., and Lawrence, G. B.: Unprocessed Atmospheric Nitrate in Waters of the Northern Forest Region in the US and Canada, *Environmental science & technology*, 53, 3620-3633, 2019.

Seibert, J., Grabs, T., Köhler, S., Laudon, H., Winterdahl, M., and Bishop, K.: Linking soil- and stream-water chemistry based on a Riparian Flow-Concentration Integration Model, *Hydrol. Earth Syst. Sci.*, 13, 2287-2297, [10.5194/hess-13-2287-2009](https://doi.org/10.5194/hess-13-2287-2009), 2009.

Seyfried, M., Lohse, K., Marks, D., Flerchinger, G., Pierson, F., and Holbrook, W. S.: Reynolds Creek Experimental Watershed and Critical Zone Observatory, *Vadose Zone Journal*, 17, 180129, [10.2136/vzj2018.07.0129](https://doi.org/10.2136/vzj2018.07.0129), 2018.

Shi, Y.: Development of a land surface hydrologic modeling and data assimilation system for the study of subsurface-land surface interaction, 2012.

Shi, Y., Davis, K. J., Duffy, C. J., and Yu, X.: Development of a coupled land surface hydrologic model and evaluation at a critical zone observatory, *Journal of Hydrometeorology*, 14, 1401-1420, 2013.

Shi, Y., Eissenstat, D. M., He, Y., and Davis, K. J.: Using a spatially-distributed hydrologic biogeochemistry model with a nitrogen transport module to study the spatial variation of carbon processes in a Critical Zone Observatory, *Ecological Modelling*, 380, 8-21, 2018.

Skamarock, W., and Klemp, J.: A Description of the Advanced Research WRF Model Version 4. Ncar Technical Notes, No, NCAR/TN-556+ STR, 2019.

Song, X., Zhang, J., Zhan, C., Xuan, Y., Ye, M., and Xu, C.: Global sensitivity analysis in hydrological modeling: Review of concepts, methods, theoretical framework, and applications, *Journal of hydrology*, 523, 739-757, 2015.

Steefel, C., Appelo, C., Arora, B., Jacques, D., Kalbacher, T., Kolditz, O., Lagneau, V., Lichtner, P., Mayer, K. U., and Meeussen, J.: Reactive transport codes for subsurface environmental simulation, *Computational Geosciences*, 19, 445-478, 2015.

1088 Steefel, C. I., and Lasaga, A. C.: A coupled model for transport of multiple chemical species and kinetic  
1089 precipitation/dissolution reactions with application to reactive flow in single phase hydrothermal systems,  
1090 American Journal of science, 294, 529-592, 1994.

1091 Steimke, A. L., Han, B., Brandt, J. S., and Flores, A. N.: Climate change and curtailment: Evaluating water  
1092 management practices in the context of changing runoff regimes in a snowmelt-dominated basin, Water,  
1093 10, 1490, 2018.

1094 Sullivan, P. L., Hynek, S. A., Gu, X., Singha, K., White, T., West, N., Kim, H., Clarke, B., Kirby, E., Duffy, C.,  
1095 and Brantley, S. L.: Oxidative dissolution under the channel leads geomorphological evolution at the Shale  
1096 Hills catchment, American Journal of Science, 316, 981-1026, 10.2475/10.2016.02, 2016.

1097 Suseela, V., Conant, R. T., Wallenstein, M. D., and Dukes, J. S.: Effects of soil moisture on the temperature  
1098 sensitivity of heterotrophic respiration vary seasonally in an old - field climate change experiment, Global  
1099 Change Biology, 18, 336-348, 2012.

1100 Taylor, R. G., Scanlon, B., Döll, P., Rodell, M., Van Beek, R., Wada, Y., Longuevergne, L., Leblanc, M.,  
1101 Famiglietti, J. S., and Edmunds, M.: Ground water and climate change, Nature climate change, 3, 322,  
1102 2013.

1103 Todd, D. K., and Mays, L. W.: Groundwater Hydrology, Welly Inte, 2005.

1104 van der Velde, Y., de Rooij, G. H., Rozemeijer, J. C., van Geer, F. C., and Broers, H. P.: Nitrate response of  
1105 a lowland catchment: On the relation between stream concentration and travel time distribution  
1106 dynamics, Water Resources Research, 46, 10.1029/2010wr009105, 2010.

1107 van der Velde, Y., Vercauteren, N., Jaramillo, F., Dekker, S. C., Destouni, G., and Lyon, S. W.: Exploring  
1108 hydroclimatic change disparity via the Budyko framework, Hydrological Processes, 28, 4110-4118,  
1109 10.1002/hyp.9949, 2014.

1110 Weiler, M., and McDonnell, J. R. J.: Testing nutrient flushing hypotheses at the hillslope scale: A virtual  
1111 experiment approach, J. Hydrol., 319, 339-356, 10.1016/j.jhydrol.2005.06.040, 2006.

1112 Weitzman, J. N., and Kaye, J. P.: Nitrogen Budget and Topographic Controls on Nitrous Oxide in a Shale -  
1113 Based Watershed, Journal of Geophysical Research: Biogeosciences, 123, 1888-1908, 2018.

1114 Wen, H., Perdrial, J., Bernal, S., Abbott, B. W., Dupas, R., Godsey, S. E., Harpold, A., Rizzo, D., Underwood,  
1115 K., and Adler, T.: Temperature controls production but hydrology controls export of dissolved organic  
1116 carbon at the catchment scale, 24, 945-966, 2020.

1117 Wieder, W. R., Allison, S. D., Davidson, E. A., Georgiou, K., Hararuk, O., He, Y., Hopkins, F., Luo, Y., Smith,  
1118 M. J., and Sulman, B.: Explicitly representing soil microbial processes in Earth system models, Global  
1119 Biogeochemical Cycles, 29, 1782-1800, 2015.

1120 Winter, T., Harvey, J., Franke, O., and Alley, W.: Natural processes of ground-water and surface-water  
1121 interaction, Ground Water and Surface Water: A Single Resource, US Geological Survey Circular, 1139, 2-  
1122 50, 1998.

1123 Wolery, T. J.: EQ3/6, a software package for geochemical modeling of aqueous systems: package overview  
1124 and installation guide (version 7.0), 1992.

1125 Xiao, D., Shi, Y., Brantley, S. L., Forsythe, B., DiBiase, R., Davis, K., and Li, L.: Streamflow Generation From  
1126 Catchments of Contrasting Lithologies: The Role of Soil Properties, Topography, and Catchment Size,  
1127 Water Resources Research, n/a, 10.1029/2018wr023736, 2019.

1128 Yan, Q., Duan, Z., Mao, J., Li, X., and Dong, F.: Effects of root-zone temperature and N, P, and K supplies  
1129 on nutrient uptake of cucumber (*Cucumis sativus* L.) seedlings in hydroponics, Soil Science and Plant  
1130 Nutrition, 58, 707-717, 2012.

1131 Yan, Z., Bond-Lamberty, B., Todd-Brown, K. E., Bailey, V. L., Li, S., Liu, C., and Liu, C.: A moisture function  
1132 of soil heterotrophic respiration that incorporates microscale processes, Nat Commun, 9, 2562,  
1133 10.1038/s41467-018-04971-6, 2018.

1134 Zarnetske, J. P., Bouda, M., Abbott, B. W., Saiers, J., and Raymond, P. A.: Generality of hydrologic transport  
 1135 limitation of watershed organic carbon flux across ecoregions of the United States, *Geophysical Research*  
 1136 *Letters*, 45, 11,702-711,711, 2018.  
 1137 Zhi, W., Li, L., Dong, W., Brown, W., Kaye, J., Steefel, C., and Williams, K. H.: Distinct Source Water  
 1138 Chemistry Shapes Contrasting Concentration-Discharge Patterns, *Water Resources Research*, 55, 4233-  
 1139 4251, 10.1029/2018wr024257, 2019.  
 1140 Zhi, W., and Li, L.: The Shallow and Deep Hypothesis: Subsurface Vertical Chemical Contrasts Shape Nitrate  
 1141 Export Patterns from Different Land Uses, *Environmental Science & Technology*, 54, 11915-11928,  
 1142 10.1021/acs.est.0c01340, 2020.  
 1143 Zhi, W., Williams, K. H., Carroll, R. W. H., Brown, W., Dong, W., Kerins, D., and Li, L.: Significant stream  
 1144 chemistry response to temperature variations in a high-elevation mountain watershed, *Communications*  
 1145 *Earth & Environment*, 1, 10.1038/s43247-020-00039-w, 2020.  
 1146 Zhou, T., Shi, P., Hui, D., and Luo, Y.: Global pattern of temperature sensitivity of soil heterotrophic  
 1147 respiration (Q<sub>10</sub>) and its implications for carbon - climate feedback, *Journal of Geophysical Research:*  
 1148 *Biogeosciences*, 114, 2009.  
 1149  
 1150  
 1151